2014-01-27

On the Transition of Non-Newtonian Blood Analogs in Straight and Stenosed Pipe Flow

Li, Lin

UNIVERSITY OF CALGARY

On the Transition of Non-Newtonian Blood Analogs in Straight and Stenosed Pipe Flow

by

Lin LI

A THESIS

SUBMITTED TO THE FACULTY OF GRADUATE STUDIES

IN PARTIAL FULFILMENT OF THE REQUIREMENTS FOR THE

DEGREE OF MASTER OF SCIENCE

BIOMEDICAL ENGINEERING GRADUATE PROGRAM

CALGARY, ALBERTA

January, 2014

Abstract

The non-linear viscous assumption of blood is evaluated through the use of an aqueous xanthan gum blood analog compared to a commonly used Newtonian analog in *in vitro* models of healthy and stenotic arteries. Pressure drop of unobstructed steady, unsteady, and post-stenotic flows were measured across laminar, transitional and turbulent regimes of Newtonian pipe flow. Results have shown that the non-Newtonian blood analog could delay the onset of transition and extend laminar flow behaviour to a Reynolds number of 3200 which showed on a macroscale level a good agreement with porcine blood. Subsequently, similar delayed transition was observed for unsteady flow at Womersley numbers of 4 and 6. For post-stenotic flows, the Newtonian to non-Newtonian minor loss ratios were lower than the unobstructed arterial model ratios, suggesting an elongation of the recirculation region for the non-Newtonian analog. These findings indicate the importance of the non-Newtonian viscous behaviour of blood on the resultant flow behaviour and cardiovascular pathologies in such environments.

Acknowledgements

First, I want to express my gratitude to Dr. David Rival for taking me under supervision to pursue my master's degree in Biomedical Engineering graduate program. I have found great illumination and strong encouragement in every talk we had during my graduate study, without which I could not have handled everything smoothly as a first time international student. I am also most grateful to Dr. Andrew Walker for his valuable guidance and extreme patience during my research. I feel so fortunate to have him helping and instructing me throughout my research as I could not have accomplished this study alone. I have had great pleasure in working with other members in the lab who have also been very helpful to me and with whom I will maintain friendship moving forward. Finally, I wish to thank my family and friends for their unwavering support in my overseas study at the University of Calgary.

Table of Contents

List of Figures

List of Symbols, Abbreviations and Nomenclature

Symbol	Definition
D	Pipe diameter [cm]
EC	Endothelial cell
f	Darcy friction factor [-]
Le	Entrance length [m]
L	Test pipe length [m]
ΔP	Pressure difference over test pipe section [Pa]
Q	Volumetric flow rate [$m^3\ s^{-1}$ or $L\ s^{-1}$]
R	Pipe radius [m]
Re	Reynolds number [-]
Re_{cr}	Critical Reynolds number [-]
Re_m	Mean Reynolds number [-]
Re_{os}	Oscillatory Reynolds number [-]
U	Average/bulk velocity [$m\ s^{-1}$]
u_m	Mean velocity component [$m\ s^{-1}$]
u_{os}	Oscillatory velocity component [$m\ s^{-1}$]
AR	Amplitude ratio [-]
WSS	Wall shear stress [Pa]
ρ	Density of fluid [$kg\ m^{-3}$]
ω	Angular velocity [$rad\ s^{-1}$]
α	Womersley number [-]
μ	Dynamic viscosity [Pa s or centipoise (cP)]
μ_c	Corrected viscosity [Pa s or centipoise (cP)]
γ_a	Apparent shear strain rate [1/s]
γ_c	Corrected shear strain rate [1/s]
τ	Wall shear stress [Pa]

Chapter One: Background

In this chapter, the background of this study along with a literature review are presented. Four subsections are introduced in sequence as follows: relationship of flow characteristics and vascular tone, laminar-turbulent transition, non-Newtonian effects on flow behaviour and post-stenotic flow field.

1.1 Relationship of Flow Characteristics and Vascular Tone

Atherosclerosis and the resultant partial occlusion of the artery is one of the most frequently occurring diseases in man. Blockage or partial blockage of the carotid, the main vessel supplying blood to the brain, can lead to a stroke, which is the third largest cause of death and the largest cause of long-term disability in the western world; see Geoghegan et al. (2011). In the coronary artery, the main vessel supplying blood to the heart, high-grade stenosis with severe blockage of the arterial lumen leads to heart attacks; see Pralhad and Schultz (2004). Arterial stenosis develops by the accumulation of low-density lipoprotein (e.g. cholesterol) beneath the endothelial cell (EC) layer of the arterial wall as noted by Sherwin and Blackburn (2005). As the amount of this fatty material accumulates, there is an accompanying proliferation of connective tissue and a thickened area (plaque) forms in the vessel wall.

Hemodynamic factors, among many other causative factors, have been cited as playing a major role in the development of arterial lesions by numerous researchers; see Aoki et al. (1969), Chien (1970), Mills et al. (1970), Smith et al. (1972), Young and Tsai (1973a, b), Yee et al. (2008). Pressure field and wall shear stress (WSS) patterns associated with blood flow through arteries are closely linked to ECs' physiological functions: ECs directly sense their mechanical environment and trigger a cascade of biochemical signals to reorganize across molecular, cellular,

tissue, and system levels, as noted by Taylor and Draney (2004) and Yee et al. (2008). Therefore, the assessment of blood flow is fundamental to the understanding, prevention, detection and treatment of cardiovascular diseases.

Although normal and healthy cardiovascular flow is accepted to be predominantly laminar under resting conditions, many forms of cardiovascular disease such as atherosclerosis and post-stenotic dilatation are associated with turbulent blood flow; see Smith et al. (1972), Stein and Sabbah (1976), Yee et al. (2008). Turbulent flow gives rise to low and oscillatory shear stress that has detrimental consequences to vascular homeostasis by contributing to thrombosis, augmenting the sickling process, damaging the EC layer and decreasing nitric oxide production; see Fry (1968), Smith et al. (1972), Stein et al. (1976), Yee et al. (2008). Moreover, the increased energy dissipation associated with turbulent flow would increase the pressure drop along arteries and result in an increased heart-pumping load; see Nichols and O'Rourke (2005). Thus, transitional and turbulent flow is not desirable in the blood circulation. With this in mind, a better understanding and an accurate prediction of laminar-turbulent transition is essential in order to control or avoid the onset of detrimental turbulent blood flow in the cardiovascular system.

1.2 Laminar-Turbulent Transition

The laminar-turbulent transition process refers to the intermediate changeover of fluid motion from a smooth laminar state to a fluctuating and agitated turbulent state; see White (2010). Turbulent flow is characterized by three-dimensional, unsteady fluctuations in velocity, temperature and concentration of the fluid particles; see Draad et al. (1998), Smits (2010). Ever since Osborne Reynolds's original dye experiments on flow transition, there has been persistent research done on elucidating the nature and origin of this process; see Willis et al. (2008),

Eckhardt (2009), Mullin (2011). Yet more than a hundred years later, much is still unknown about the seemingly simple question of when and how the flow within an ordinary pipe turns turbulent. In hemodynamic research, pipe flow transition gained attention not only due to its fundamental role in fluid mechanics, but also the widespread applications of pipe flow systems in the *in vitro* modelling of the human cardiovascular system.

A significant body of research has been completed on the transitional regime of pipe flow for Newtonian fluids whose viscosity is independent of the shear strain rate; see Mullin (2011). It is already well-established that this critical point from laminar to turbulence is dependent on a dimensionless parameter termed the Reynolds number (*Re*). With the increase of *Re*, natural transition occurs when there are no external sources of disturbances deliberately introduced into the system; see Mullin (2011). Experimental studies carried out by Wygnanski and Champagne (1973), Darbyshire and Mullin (1995) and Hof et al.(2003) have shown that two kinds of distinct turbulent patches appear within the intermittent natural transition process, which are known as puffs (at lower *Re* in transitional regime) and slugs (at higher *Re* in transitional regime). In the case of puffs, they co-exist with the surrounding laminar flow and decay as they propagate downstream; see Eckhardt et al. (2007). In the case of slugs, there is no re-laminarization process and they grow to fully developed turbulence across the entire pipe; see Wygnanski and Champagne (1973). The natural transition process, if it is the mechanism for turbulence production in the circulatory system, should have an important influence on the force–vessel wall interactions through high-frequency fluctuations in pressure and WSS; see Nichols and O'Rourke. (2005).

When pulsatile flow is considered, the problem becomes more complex. It is seen in the literature that the authors do not agree on the criterion for transition in pulsatile flow: Hershey

and Im (1968) proposed that transition occurs at a lower critical time-averaged mean *Re* (Re_m) than would be expected in steady flow since pulsatile flow is inherently more unstable. However, according to Sarpkaya (1966), the critical *Re* (Re_{cr}) at which laminar flow can no longer be maintained for pulsatile flow is higher compared to steady flow. Aside from Re_m, Womersley number (α) is another dimensionless parameter used to characterize pulsatile flow and has raised disagreements on its influence in transition. Nerem and Seed (1972), Einav and Sokolov (1993) and Peacock et al. (1998) all suggested a correlation for the initiation of turbulence to α whereupon Re_{cr} increases with larger α while Sarpkaya (1966) and Hershey and Im (1968) indicated the opposite trend. Trip et al. (2012) systematically investigated transitional sinusoidal pulsatile flows at $\alpha > 10$ and reported that transition is only dependent on Re_m and neither α nor the oscillatory *Re* (Re_{os}) has an influence. Stettler and Hussain (1986) drew similar conclusions for $\alpha > 10$ where pulsatility was found to have little influence on Re_{cr}. However, they identified another region between $4 < \alpha < 8$ where clear conclusions are still lacking. Unfortunately, this region is of primary interest in hemodynamic research given that several arteries at resting heart rate (~1 Hz) present with α in this range; see Pedley et al. (2011). In this study, I seek to address this shortcoming by acquiring pulsatile measurements in this region of uncertainty and physiological relevance between $4 < \alpha < 8$.

1.3 Non-Newtonian Effects on Flow Behaviour

Compared to research with Newtonian fluids, less attention has been given to the non-Newtonian effects on flow behaviour despite the fact that most of the frequently encountered fluids in engineering are non-Newtonian; see Draad et al. (1998). The demand for studying real fluids used in chemical, pharmaceutical, food and biomedical industries is increasing due to the

severe limitations in the application of ideal and Newtonian flow theories to flow problems in these aspects; see Pak et al. (1991). Non-Newtonian fluids exhibit shear-dependent viscosities that are no longer constant over different shear strain rates as with Newtonian fluids. Previous studies on non-Newtonian fluids revealed contradictory results in that transition to turbulence could occur at lower, roughly the same or higher *Re* compared to Newtonian fluids in matching conditions; see Dodge et al. (1959), Virk et al. (1966), Chung and Graebel (1972), Zakin et al. (1977). However, the working fluids used in these studies were polymer solutions exhibiting highly elastic behaviour in relation to blood.

More specifically, blood is a shear-thinning, incompressible, visco-elastic non-Newtonian fluid due to its complex composition; see Pedley (1980), Nichols and O'Rourke (2005), Pedley et al. (2011). It also exhibits yield stress characteristic below which no flow is induced; see Mejia et al. (2012). From a mechanical point of view, whole blood may be regarded as consisting of flexible and deformable red blood cells suspended in Newtonian plasma as noted by Nichols and O'Rourke (2005). It is these red blood cells that are partly responsible for the non-Newtonian behaviour of blood including shear-thinning and viscoelasticity; see Gijsen et al. (1999), Han et al. (2001). However, the complexity of the non-Newtonian consideration is one of the reasons that blood is often assumed to be Newtonian and homogeneous. The viscosity of blood is usually taken as the high shear strain rate value of 3.5 centipoise (cP) since the shear strain rate in large arteries is believed to be high enough for blood rheology to be assumed linear; see Gijsen et al. (1999), Mejia et al. (2011), Pedley et al. (2011). Various mathematical models have been proposed to simulate the rheology of blood, (e.g. power law and Bird-Carreau-Yasuda model; see Draad et al. (1998)), but none of these models has been accepted as the true reflection of whole blood behaviour; see Cho and Kensey (1990), Ballyk et al. (1994). Among the

computational studies, it still remains contentious whether the non-linear viscous behaviour of blood plays an important role in quantifying blood flows. Johnston et al. (2006) compared both Newtonian and non-Newtonian models of blood and found it reasonable to use the former assumption in evaluating shear stress in the coronary artery. Tang et al. (2004) suggested that the non-Newtonian effect of blood is among the factors of lowest order of importance in predicting stenotic arterial blood flow. A similar suggestion was proposed by Gonzalez et al. (2005) who only found a 1% difference in the prediction of unsteady WSS between two non-Newtonian models and a 5% difference between Newtonian and non-Newtonian models of blood. On the other hand, the translation of the Newtonian assumption of blood in the already complicated question of laminar-turbulent transition, as well as low and oscillating shear flows downstream of a constriction may poorly reflect true blood behaviour. Mejia et al. (2011) discovered through computational fluid dynamics (CFD) that the Newtonian assumption underestimates WSS and overestimates the risk for atherosclerosis, and that non-linear rheological models result in a more accurate prediction of WSS in a stented arterial segment. Similar conclusions were reached by Schirmer and Malek (2007) and Liu et al. (2011) on the overestimation of low WSS regions by Newtonian assumptions. However, the choice of parameters for inclusion in non-Newtonian models could greatly change the outcome for numerical modeling, as noted by Hron et al. (2000), Razavi et al. (2011).

In order to illustrate true blood behaviour in such environments, it is ideal to use real blood in experimental investigations. However, due to practical reasons (e.g. limited access and difficulty for storage and handling), blood analog fluids are often utilized instead of real blood when undertaking *in vitro* experiments. Similar to past experimental work, the blood analog fluids used in this study were constructed by dissolving xanthan gum in aqueous glycerol to

replicate whole blood behaviour; see Gijsen et al. (1999), Walker et al. (2012, 2013). The xanthan gum solution follows that suggested by Brookshier and Tarbell (1993), who reported that the xanthan gum analog provides a good approximation of the visco-elastic behaviour of porcine blood by measuring wall shear strain rate waveforms over a board range of shear strain rates and hematocrit levels. In an earlier study, Brookshier and Tarbell (1991) found that the viscous behaviour of porcine blood closely matched that of human blood. However, their evaluation of the blood analog fluid with respect to porcine blood was restricted to laminar flow conditions (max Re = 1600). To my knowledge, research is still lacking in the characterization of non-Newtonian and Newtonian blood analog fluids in experimental steady and pulsatile transitional flows whereupon my work seeks to assess the influence of the non-linear viscous effects on different transition mechanisms.

1.4 Post-stenotic Flow Field

Regardless of the cause of the arterial stenosis, it is evident that once a blockage has formed within the vessel, the post-stenotic blood flow will be disturbed and the hemodynamic factors in turn will play an increasingly important role in the development of the disease as noted by Nichols and O'Rourke (2005). The following hemodynamic factors are believed to have biological relevance to the stenosis progression: (1) the resistance of the stenosis, characterized by the relationship between the pressure drop and flow; see Young et al. (1973a); (2) the distribution of pressure and WSS through the stenosis; see Fry (1968); (3) the extent of localized separated regions of flow; see Fox and Hugh (1966) and (4) the extent and intensity of turbulence developed at the stenosis; see Sawyer (1965).

The possibility of generating transitional and turbulent flow is greatly increased by the presence of a constriction. The high velocity fluid entering the constriction due to reduced vascular cross-sectional area causes a jet to form at the exit of the constriction due to sudden expansion. Zadrazil et al. (2012) and Geoghegan et al. (2013) have shown that two distinct flow regions exist downstream of the constriction including a high velocity/momentum jet close to the centerline and a low velocity/momentum recirculating flow region near the wall. These two regions are separated by a shear layer with a high spatial velocity gradient that produced a Kelvin-Helmholtz vortex ring system further downstream; see Geoghegan et al. (2013). The shear layer generated by a constriction detaches from the wall and becomes turbulent even at a very low *Re* depending on the severity of the stenosis; see Mittal et al. (2001), Vetel et al. (2008). The shear layer induced turbulence downstream of an arterial stenosis can cause a large pressure drop and create an adverse mechanical environment to the downstream arterial wall by generating separation, recirculation and reattachment regions with atherogenic low and oscillatory WSS and shear strain rates; see Peilhop et al. (2012). When combined with flow pulsatility, the investigation becomes even more complicated aside from the already present complex flow features seen in a steady post-stenotic flow. In general, transition is believed to occur in constricted tubes at relatively small $Re_{cr,}$ which is well below the Re_{cr} for flow in a straight, unobstructed pipe; see Young and Tsai (1973a, b).

The conditions under which laminar or turbulent flow can exist in the cardiovascular system have long been of concern to researchers; see Hershey and Im (1968). Under normal resting conditions in humans, flow in the proximal aorta is turbulent as noted by Nichols and O'Rourke (2005). However, there is still no clear evidence as to what triggers turbulence production in the cardiovascular system – the natural transition process or a shear layer induced turbulence

production, the former resulting from upstream perturbations and the latter from local disturbances in the wall region; see Nichols and O'Rourke (2005). Therefore, it is important to investigate on the different turbulence production mechanisms in order to better understand and optimize the treatment of atherosclerosis. A complete understanding of the relationship between pressure, flow and symptoms for arterial stenosis can be used to predict and alter the blood flow to change the course of disease as noted by Varghese et al. (2007). Furthermore, in the investigation of the shear layer induced turbulent post-stenotic flow, the inclusion of non-Newtonian viscous behaviour has been minimal. One such study including non-Newtonian consideration in post-stenotic flow was carried out by Walker et al. (2013) using an aqueous xanthan gum solution. It was found that the high velocity fluctuations were dampened by the non-Newtonian fluid, which implied the importance of the non-linear viscous assumption of blood in evaluating the post-stenotic flow field. Therefore, I seek to experimentally quantify how the viscous assumptions of two blood analogs (Newtonian and non-Newtonian) affect the processes of natural and shear layer induced turbulence.

1.5 Outline of the Thesis

In Chapter Two, the aims and hypotheses of the study are outlined on the steady, pulsatile and stenotic flow of Newtonian and non-Newtonian blood analogs. The measurement techniques and experimental setup to be used, as well as the characterization of the non-Newtonian analog are described in Chapter Three. The results of steady, pulsatile and stenotic pipe flow along with the discussions are presented in Chapter Four. The final chapter of this thesis, Chapter Five, will summarize my main conclusions and recommendations for future research.

Chapter Two: Study Aims and Hypotheses

Based on the literature review presented, the objectives of the study are introduced in this chapter. The study aims and hypotheses are divided into three subsections regarding steady, pulsatile and post-stenotic flow, respectively.

2.1 Steady Flow

Based on the findings of Han et al. (2001), circulating porcine blood displayed prolonged laminar flow behaviour until a *Re* of ~ 3200, which is beyond the commonly accepted critical value of 2300 for the onset of transition in steady pipe flow. Han et al. (2001) attributed this phenomenon to the visco-elastic nature of red blood cells, which could dampen the disturbances in turbulent flow. However, due to the complexities in handling and experimenting with real blood, *in vitro* hemodynamic model studies often rely on analog fluids that replicate blood's rheological properties. To date, the majority of studies have used Newtonian fluids, despite the fact that blood is non-Newtonian, shear-thinning and viscoelastic in nature. Brookshier and Tarbell (1993) discovered that the behaviour of an aqueous solution of xanthan gum in glycerol could provide a good approximation of the shear-thinning and visco-elastic properties of porcine blood. However, their characterizations were restricted within the laminar regime to a *Re* of 1600. Building upon the work of Brookshier and Tarbell (1993), the first aim of this study was to expand the evaluation of the non-Newtonian blood analog up to transitional and turbulent regimes. I hypothesize, that the non-Newtonian analog will delay the onset of transition to a comparable Re_{cr} observed for porcine blood since it is suggested that the added xanthan gum serves to dampen the turbulent bursts by possessing a similar rheological behaviour to that of red

blood cells. To test this hypothesis, pressure drop measurements were acquired between two pressure taps placed on a straight, unobstructed acrylic tube section. Both a commonly used Newtonian analog fluid consisting of a glycerol-water mixture and an aqueous xanthan gum solution mimicking whole blood behaviour were circulated through a closed flow loop in steady conditions up to a $Re \sim 7600$. Direct comparisons were made to quantify the onset of transitional behaviour between the two analog fluids by constructing plots of pressure drop as a function of *Re* and Moody diagrams. It is expected that this finding will not only validate the suitability of using the analog fluid suggested by Brookshier and Tarbell (1993) in modelling transitional and turbulent blood flow, but also advocate the importance of non-Newtonian viscous considerations in that a delayed transition is observed.

2.2 Pulsatile Flow

For unsteady flow studies, Trip et al (2012) conducted a systematic investigation on transitional pulsatile pipe flow of a Newtonian fluid. It was concluded that similar to steady flow, only *Re* is the determinant parameter for the onset of transition for pulsatile flow and neither α nor Re_{os} are relevant. However, the experiments of Trip et al. (2012) were limited to $\alpha > 10$ where other studies have also demonstrated that these values have little influence on the Re_{cr}; see Stettler and Hussain (1986). These studies have identified a α region between 4 and 8 where uncertainty still remains on the relationship between α and the initiation of transition, as noted by Trip et al. (2012). It should be noted that these studies are associated with the use of Newtonian fluid. This gives rise to the second aim of my study, which is to quantitatively evaluate the relationship between transition and pulsatility at $4 < \alpha < 8$ using both Newtonian and non-Newtonian analog fluids. I hypothesize, that transition to turbulence will be delayed for both

fluids at higher α since the time in each cycle for generating turbulent bursts is shorter at higher pulsatile frequency. Furthermore, it is hypothesized that the non-Newtonian viscous effect will serve to dampen turbulent bursts, as in steady flow, leading to an extension of laminar flow behaviour to a higher Re_{cr} than the Newtonian analog. To test this hypothesis, pressure drop measurements were acquired between two pressure taps located on a straight unobstructed acrylic pipe under pulsatile conditions. The Re_{os} for unsteady measurements was set to 1/3rd of the Re_m. The maximum Re_m quantified for both fluids was 5600 that equated to a peak Re of ~7600. For each pulsatile waveform at each Re_m, three waveforms at α of 4, 6 and 8 were constructed and pressure drop measurements acquired. To analyze the data, separate plots of pressure drop as a function of Re_m and Moody diagrams were presented at each α to allow direct comparisons for the initiation of transition in relation to pulsatile frequency for both analog fluids.

2.3 Shear Layer Induced Transitional Flow

Investigations into transitional and turbulent flow downstream of a pipe constriction have been well documented; see Blackburn and Sherwin (2007). The formation of separated strong shear layers have been demonstrated to be susceptible to convective instabilities for Newtonian fluids, as noted by Blackburn et al. (2008). Shear layer induced instabilities, as a comparison to natural transition in the unobstructed pipe, provided the motivation for the third aim of my study whereupon I seek to evaluate the stenotic induced pressure drops in relation to the viscous behaviour of the circulating fluids. As mentioned previously, studies quantifying blood flow, including the post-stenotic flow field, have largely relied upon the use of a Newtonian assumption for blood. One such experimental study that incorporated the non-Newtonian viscous

consideration was carried out by Pak et al. (1990) in a sudden expansion pipe. It was found that in turbulent flow, the non-Newtonian visco-elastic fluid expanded the downstream recirculation length three times longer than that for water. Similarly, Walker et al. (2013) found that the recirculation length was extended for the non-Newtonian analog at the peak of their pulsatile flow at an inlet Re_m ~1250 and $\alpha \sim 4.4$. Furthermore, given the relationship between recirculation and energy dissipation suggested by the studies of Bullen et al. (1988), Fossa and Guglielmini (2002) and Fratino and Pagano (2011), it is hypothesized that the ratio of the stenotic induced pressure drop (minor loss) of the Newtonian analog to that of the non-Newtonian analog is lower than the natural transition pressure drop ratios due to the non-Newtonian elongation of the recirculation region. To test this hypothesis, a brass hex nipple was threaded to the end of the unobstructed measurement section to model an axi-symmetric stenotic constriction with a 44 % area reduction. A second piece of acrylic tube was attached to the other end of the hex nipple and an additional pressure tap was placed at 36 pipe diameters (D) downstream of the constriction outlet. Pressure drop measurements were performed in both steady and pulsatile flows with dynamic parameters commensurate with my previous work. The minor losses were found by subtracting the extended unobstructed system pressure drops acquired in the first study aim from the total stenotic system pressure drops acquired upon the addition of the constriction. It is expected that this work will show analogous behaviour of the non-Newtonian fluid as hypothesized in my previous study aims whereupon a decrease in the total obstructed system pressure drop will be observed. The different ratios of the two analogs in relation to the transitional mechanism would imply the importance of non-linear viscous assumptions in evaluating the post-stenotic flow field.

Chapter Three: Materials and Methods

In this chapter, the experimental setup for the pressure drop measurements will be described. Special attention is given to the rheological characterization of the non-Newtonian blood analog.

3.1 Characterization of Working Fluids

The working blood analog fluids included a Newtonian control fluid with which viscosity is constant over all shear strain rates and a non-Newtonian analog with shear-rate dependent viscosities in laminar pipe flow. The Newtonian control analog consisted of a 12.3% by weight glycerol and 87.7% deionized water mixture to match the high shear strain rate asymptotic viscosity of the non-Newtonian fluid. The densities of the Newtonian and non-Newtonian analog fluids were 1026 kg/m^3 and 1009 kg/m^3, respectively. The viscosity of the Newtonian control fluid was taken as the average of three measurements acquired by a Cannon-Fenske routine calibrated CRFC (9271-B50) series size-50 capillary viscometer (Cannon-Fenske, PA, USA). Initial capillary viscometer measurements were completed using water as the control fluid, which represented a Newtonian fluid with known viscosity at room temperature (~ 20 ˚C). The wall shear strain rate of the Newtonian analog is determined using Equation 3.1:

$$\gamma_a = \frac{4Q}{\pi R^3} \tag{3.1}$$

where γ_a is the apparent wall shear strain rate, Q is the volumetric flow rate, and R is the pipe radius. The calculation of WSS for both fluids follows that of Equation 3.2:

$$\tau = \frac{\Delta P R}{2L} \tag{3.2}$$

where τ is the shear stress at the wall, ΔP is the pressure drop over two pressure taps, R is the radius, L is the distance between pressure taps.

For the non-Newtonian fluid, 50 mg xanthan gum was added into a 4% by weight glycerol and deionized water solution to replicate the viscoelastic and shear-thinning properties of blood as suggested by Brookshier and Tarbell (1993). To determine the rheological properties of this unknown non-Newtonian analog fluid, pressure drops were acquired across a range of shear strain rates in steady, laminar flow. Furthermore, special steps are required in the calculation of the wall shear strain rates since the near-wall velocity gradient for non-Newtonian fluids is generally larger than that of Newtonian fluids in matching flow conditions (e.g. the same flow rate, radius, etc.); see Tickner and Sacks (1969). To account for the larger near wall shear strain rate for the non-Newtonian fluid, the Weissenberg-Rabinowitsch correction (Equation 3.3) for shear strain rate is applied to the non-Newtonian analog fluid; see Tickner and Sacks (1969):

$$\gamma_c = \frac{4Q}{\pi R^3}\left[\frac{1}{4}\left(3 + \frac{d\ell n\gamma_a}{d\ell n\tau}\right)\right] \tag{3.3}$$

where γ_c is the corrected wall shear strain rate, Q is the volumetric flow rate, R the pipe radius, γ_a the apparent shear strain rate (Equation 3.1), and τ the wall shear stress as calculated by the measured pressure drop (Equation 3.2):

Final corrected viscosities (μ_c, Equation 3.4) were derived through the division of the calculated WSS (τ) and corrected wall shear strain rate (γ_c) using Equations 3.2 and 3.3, respectively:

$$\mu_c = \frac{\tau}{\gamma_c} \tag{3.4}$$

The rheological characterization of the non-Newtonian blood analog fluid used in this study is shown in Figure 3.1 whereupon wall shear strain rates for the non-Newtonian analog presented represent corrected values based on Equation 3.3. The presented normalized viscosities (μ/μ_{avg}) were derived through the division of the corrected viscosity (μ_c) of the non-Newtonian analog at each γ_c to the average viscosity of the Newtonian control fluid (μ_{avg}). In Figure 3.1, the non-Newtonian fluid demonstrated a shear-thinning behaviour and presented with a high shear strain rate viscosity of ~ 1.38 cP that closely matches the average viscosity of the Newtonian analog. It is observed that the normalized viscosities of the non-Newtonian analog fluid to its high shear strain rate value resemble those of the normalized blood viscosities to their representative high shear strain rate viscosities at several hematocrit levels; see Valant et al. (2011). Therefore, it is appropriate to assume that the non-Newtonian analog fluid could provide a good representation of whole blood behavior on a macroscale level. The shear-rate dependent viscosity relationship for the non-Newtonian analog determined from Figure 3.1 was $\mu = 3.9002\gamma_c^{-0.208}$ (R^2=0.9898). This was subsequently used as a curve fit correction to adjust the flow rate to ensure matching inlet *Re* for the analog fluids in laminar flow.

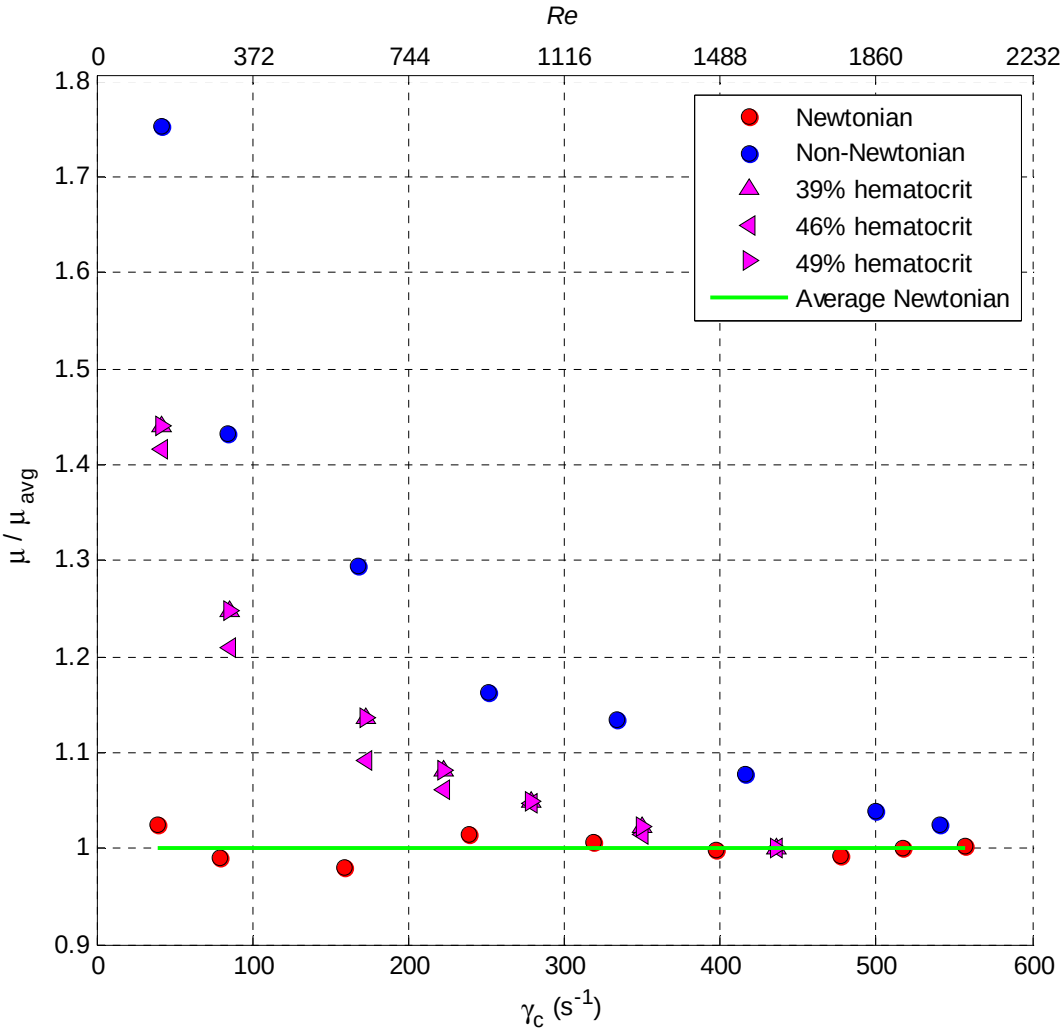

Figure 3.1 Viscous behaviour characterization of the Newtonian and non-Newtonian blood analog fluids through steady laminar pipe flow across a range of shear strain rates. Viscosities were normalized to the average viscosity of the Newtonian analog (μ/μ_{avg}). Normalized values of blood viscosities at hematocrit values of 39%, 46% and 49% to their respective high shear strain rate asymptotic viscosities are presented for reference; see Valant et al. (2011). Wall shear strain rates presented for the non-Newtonian analog fluid have been corrected using the Weissenberg-Rabinowitsch correction (Equation 3.3).

3.2 Steady Unobstructed Flow Loop Setup

In vivo arterial pressure drop and WSS measurements would be difficult to obtain considering the cost and instrumentation, particularly for human subjects. Furthermore, existing

pressure drop measurements in animals make it difficult to isolate the specific influence of the non-linear rheology on a physiological system compared to other factors such as vessel compliance and pulsatility; see Pedley et al. (2011). Consequently, the *in vitro* experimentation using models with reflection of the critical characteristics of the *in vivo* flow environments have become very useful.

In this study, a closed flow loop system was constructed to model the physiological circulatory system. The experimental flow facility is shown in Figure 3.2 as a simplified *in vitro* model of a healthy, non-stenotic artery. Analog fluids contained in the open reservoir were circulated through the loop by an ISMATEC Reglo-Z digital gear pump (Cole Parmer, Montreal, QC, Canada) using a GJN-25 Micropump pump head (Cole Parmer) at room temperature. The test section consisted of a rigid cylindrical acrylic tube (Laird Plastics, Calgary, AB, Canada) with a length *(L)* of 1.83 m and a diameter (*D)* of 0.635 cm. Two pressure taps, P_1 and P_2, were spaced a distance of 1.67 m (263 *D*) on the acrylic tube and pressure drops over that distance were measured by a membrane differential pressure transducer. The pressure sensed by the membrane differential pressure transducer is converted to a DC voltage, stabilized by a regulated power supply (Circuit Test Electronics, BC, CA) and recorded by a data acquisition system (National Instruments, Austin, TX, USA). For calibration purposes, the voltage was zeroed prior to data acquisition at each flow rate. It should be noted that although the circulatory system is difficult to fully replicate *in vitro* and decidedly more complex, the simplified model herein helps to isolate the salient influence of the specific factor, i.e. the non-linear viscous behaviour of blood, to the flow field. More details regarding the limitations of the experimental setup are discussed in Appendix 1.

(a)

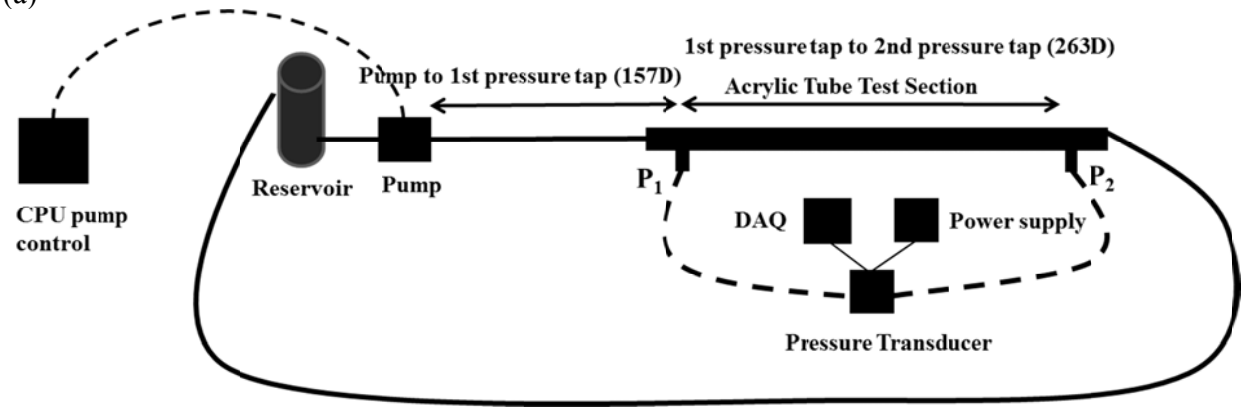

(b)

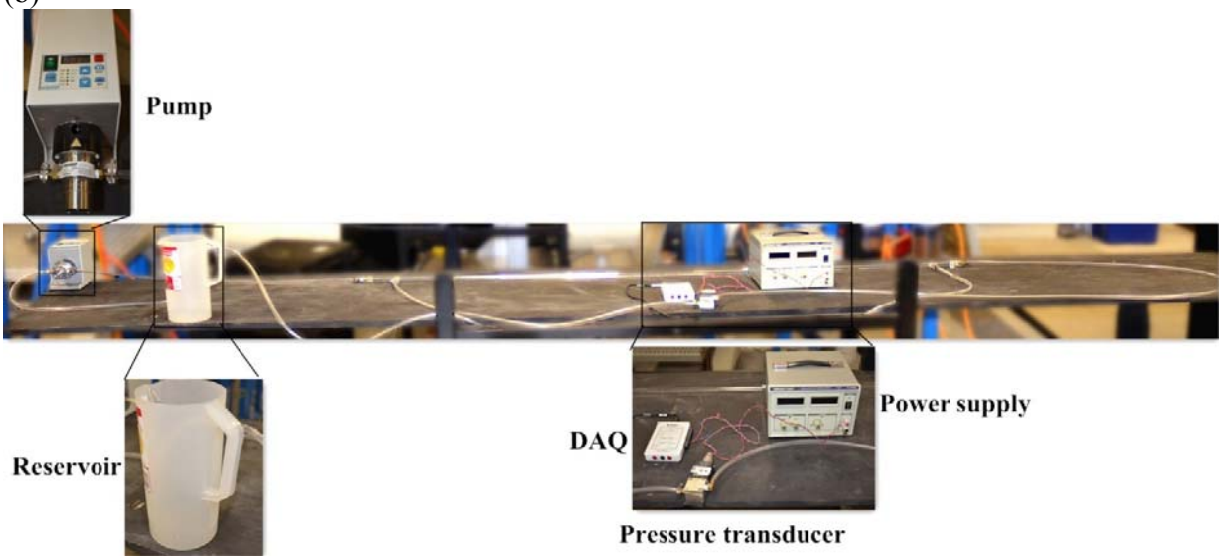

Figure 3.2 Schematic (a) and photo (b) of the flow loop for unobstructed pressure drop measurements. Note that figure (a) is not drawn to scale.

For steady pressure drop measurements, due to the inherent vibration of the pressure transducer, average values were calculated after measuring the pressure drops for approximately five seconds across four trials at a sampling frequency of 100 Hz. The viscosities of the non-Newtonian analog at $Re < 2000$ were taken and Re calculated according to the curve fit of the corresponding shear-rate dependent viscosity relationship shown in Figure 3.1. This ensured that both fluids were subjected to identical Re as defined below:

$$\mathrm{Re} = \frac{\rho \bar{U} D}{\mu} \tag{3.5}$$

where $\bar{U}$ is the average velocity (volumetric flow rate over cross-sectional area, $Q/\pi R^2$), R the diameter of the pipe, ρ the density of the working fluid and μ the dynamic viscosity. For $Re >$ 2000, viscosities of both fluids were assumed equal and thus subjected to identical flow rates; see Figure 3.1. The pressure drop over the unobstructed test section between P_1 and P_2 was measured between $400 < Re < 7600$ at selected intervals for both fluids so as to encompass the laminar, transitional and turbulent regimes of pipe flow. The Re range tested equated to a mean velocity range, assuming a viscosity of 1.38 cP of 0.085 m/s < $\bar{U}$ <1.61 m/s.

The pressure drop measurements in the laminar regime were used to validate the experimental setup and the overall procedures with the well-developed Hagen-Poiseuille's law. For laminar fully-developed Newtonian incompressible flow, the pressure drop required to drive the fluid at a certain flow rate follows that of Equation 3.6:

$$\Delta P = \frac{8 \mu L Q}{\pi R^4} \tag{3.6}$$

where R is the pipe radius, Q is the volumetric flow rate ($Q = \bar{U} \pi R^2$, where $\bar{U}$ is the average velocity of steady flow), ΔP is the pressure difference over the pipe length L, ρ is the density of the working fluid and μ is the dynamic viscosity.

In order to evaluate the behaviours of the two analog fluids in transitional and turbulent regimes, Moody diagrams were constructed to display the relationship between Darcy friction factor (f) (Equation 3.7) and Re (Equation 3.5):

$$f = \frac{\Delta P}{\rho \bar{U}^2} \frac{4R}{L} \tag{3.7}$$

where f is the Darcy friction factor, ρ is the density of the working fluid, ΔP is the pressure drop required to drive the fluid through pipe length (L) with radius (R) at an average velocity ($\bar{U}$). Three regimes of pipe flow could be determined from the Moody diagram. For the laminar regime, the pressure drop is due to viscous dissipation within the fluid such that f decreases with increasing Re by the relationship of $f = 64/Re$; see White (2011). For the turbulent regime, pressure drop is largely due to turbulent losses such that it becomes independent of Re and only a function of pipe roughness; see White (2011). The empirical Blasius relation of $f = 0.3164/Re^{1/4}$ holds for the f - Re relationship in the turbulent regime; see White (2011). Since the Blasius relation does not contain any term for pipe roughness, it is valid only for smooth pipes between $4000 < Re < 100{,}000$; see White (2011). In the transitional regime of pipe flow, f is a function of both Re and pipe roughness.

The entrance length (L_e) required for the inlet, laminar flow of the test section to be fully - developed follows that suggested by Durst *et al*. (2005):

$$\frac{L_e}{D} \approx \left[\left(0.619^{1.6}\right) + \left(0.0567\,\mathrm{Re}\right)^{1.6}\right]^{\frac{1}{1.6}} \tag{3.8}$$

where D is the diameter of the pipe and Re as defined in Equation 3.5. In turbulent flow, the boundary layers grow much faster and therefore the entrance length for achieving fully developed flow is shorter than in laminar flow. For smooth pipe walls the following equation holds:

$$\frac{L_e}{D} \approx 4.4\,\mathrm{Re}^{\frac{1}{6}} \tag{3.9}$$

where D is the diameter of the pipe, Le the required entrance length; see White (2011). For non-Newtonian fluids, Poole and Ridley (2007) concluded that the entrance lengths for Newtonian and non-Newtonian fluids are only different at $Re < 10$. However, this is much smaller than the

Re range tested in this study (400 < *Re* < 7600) and smaller than the minimum *Re* encountered (~150) in the viscous characterization of the non-Newtonian blood analog. Therefore, the 157 D entrance length used in this study ensures that the flow is fully-developed at the measurement location of P_1 for both analogs; see Figure 3.2 (a).

3.3 Unsteady Measurements

For pulsatile, unsteady measurements, the experimental setup remained unchanged from that used for steady measurements as shown in Figure 3.2 whereupon pressure drops over the unobstructed test section were measured. A simplified pulsatile waveform given by a sinusoidal varying velocity superimposed on a steady mean component was used:

$$U = U_m + U_{os} \tag{3.10}$$

where U_m is the mean steady velocity of the pulsatile flow and U_{os} is the magnitude of the oscillatory velocity. The ratio of the oscillatory to the steady component, amplitude ratio (*AR*), is also useful in describing sinusoidal pulsatile flow:

$$AR = \frac{U_{os}}{U_m} = \frac{\mathrm{Re}_{os}}{\mathrm{Re}_m} \tag{3.11}$$

Aside from Re_m, an additional dimensionless parameter is used to characterize the pulsatile flow. The Womersley number (α) describes the relative importance of the unsteady inertial forces to viscous forces:

$$\alpha = R\sqrt{\frac{\omega\rho}{\mu}} \tag{3.12}$$

where the angular frequency is defined as $\omega = 2\pi/T$ where T is the period of the pulsatile flow, μ the dynamic viscosity , R the radius of the pipe and ρ the density of working fluids. The α tested

in this study were 4, 6 and 8 at $400 < Re_m < 5600$. The entrance length for laminar oscillating pipe flow can be estimated as $Le/D=0.049Re_m$ as noted by Trip et al. (2012). Thus, the 157 D entrance length is sufficient for the flow to be considered fully developed over the parameter range tested; see Figure 3.2 (a).

The sinusoidal waveforms for pulsatile flow measurements with different α were generated using a custom designed program in NI LabVIEW 2011(National Instruments, Austin, TX, USA). One of the sinusoidal waveforms (~ 0.75 Hz) measured by an ultrasound flow meter (Transonic In., Ithaca, NY, USA) at $\alpha \sim 6$ is shown in Figure 3.3. It is believed that the use of a simplified sinusoidal waveform captures the salient features of an arterial waveform through the use of a steady flow component and minimal harmonics (see Appendix 1). The sampling frequencies were set at 100 times the specific frequency at each α in order to synchronize each cycle into 100 sampling points. Correction of inlet flow rates using the curve fit between calculated non-Newtonian viscosities and shear strain rates in Figure 3.1 ensured that both fluids were subjected to identical Re over the pulsatile cycle in the laminar regime. For $Re_m > 2000$, viscosities of both fluids were assumed equal and thus subjected to identical flow rates; see Figure 3.1. During the experiments, it was found that the sinusoidal wave frequency resonated with the inherent vibration frequency of the pressure transducer. To account for this, measured pressure drops from 15 pulsatile cycles were averaged whereupon an average pressure drop cycle across the waveform was achieved. An ideal low-pass filter was constructed using MATLAB R2010 software (MathWorks, Natick, MA) with a cut-off frequency set to 7 Hz that filtered the ringing artefact associated with the pressure transducer.

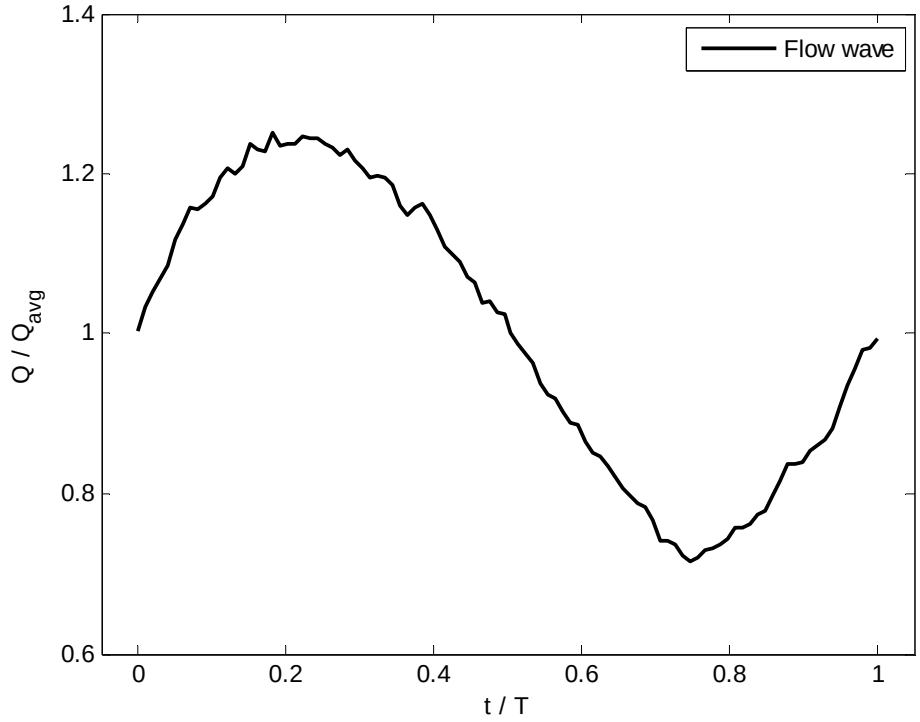

Figure 3.3 Measured pulsatile waveform (~0.75 Hz, α ~ 6) by an ultrasonic flow meter. The waveforms were generated by the digital gear pump using a custom designed program in NI LabVIEW 2011.

3.4 Obstructed Flow Loop Setup

Although the physiological arterial stenosis may be irregular in geometry, it has been frequently modeled *in vitro* using an axi-symmetric constriction inside a pipe since this configuration creates flow separation, recirculation and reattachment regions that are commonly associated with *in vivo* stenoses; see Young and Tsai (1973a), Ojha et al. (1989), Cavalcanti et al. (1995).

In this study, a brass hex nipple (Swagelok, Germany) was threaded to the 263*D* unobstructed test section to model an idealized axisymmetric arterial stenosis. The hex nipple formed a 44% area reduction at a distance of 284*D* from the first pressure tap (Figure 3.4 (c)). A

second piece of acrylic pipe was threaded to the other end of the brass hex nipple with an additional pressure tap (P_3) located at a distance of 36 D downstream from the end of the brass nipple. The distance between pressure taps P_1 and P_3 was 320 D. A schematic and photo of the experimental setup along with the dimensions of the hex nipple are shown in Figure 3.4. Again, a number of simplifications are taken to model the arterial stenosis. However, it is felt that the use of an axi-symmetric constriction to model an arterial stenosis does not diminish the validity or importance of this study (see Appendix 1).

Both steady and pulsatile pressure drop measurements were acquired to determine the total system pressure drop between P_1 and P_3. The added pressure drop to the system as a result of blockage inclusion was calculated through a two-step process. First, the unobstructed pressure drop measurements acquired between P_1 and P_2 were linearly increased by 21.5% that represented the percentage of additional length between P_2 and P_3 that was added to the total system length for stenotic pressure drop measurements. This linear increase in measurements represented expected values had unobstructed pressure drop measurements been acquired between P_1 and P_3:

$$\Delta P_n = \frac{L_{13}}{L_{12}}\left(P_2 - P_1\right) \tag{3.13}$$

where ΔP_n is the expected pressure drop if unobstructed measurements were acquired between P_1 and P_3, L_{13} is the distance between P_1 and P_3 (320 D), and L_{12} is the distance between P_1 and P_2 (263 D). Second, to calculate the additional pressure drop due to the added constriction (minor loss) to the overall system, linearly extended unobstructed pressure drops were simply subtracted from the total system stenotic pressure drops:

$$\Delta P_c = \Delta P_s - \Delta P_n \tag{3.14}$$

where ΔP_c is the pressure drop due to the added constriction and the associated shear layer induced convective instabilities, ΔP_s is the total obstructed system pressure drop and ΔP_n is the expected calculated pressure drop upon extension of the unobstructed pressure drop measurements between P_1 and P_3 (Equation 3.13). The parameters and measurement techniques used in the obstructed flow loop are commensurate with the unobstructed flow loop as described previously in both steady and pulsatile flows and thus are not described here again. The presentation of the obstructed flow data are based on both inlet *Re* (Re_{in}) and stenotic *Re* (Re_{st}) as defined below:

$$\mathrm{Re}_{in} = \frac{\rho \overline{U}_{in} D}{\mu} \tag{3.15}$$

$$\mathrm{Re}_{st} = \frac{\rho \overline{U}_{st} (0.75) D}{\mu} \tag{3.16}$$

where ρ is the density of the fluids, $\overline{U}_{in}$ and $\overline{U}_{st}$ are average inlet and stenotic velocities, respectively, μ is the (corrected) viscosity and 0.75 is the proportion of the stenosis D to the pipe D.

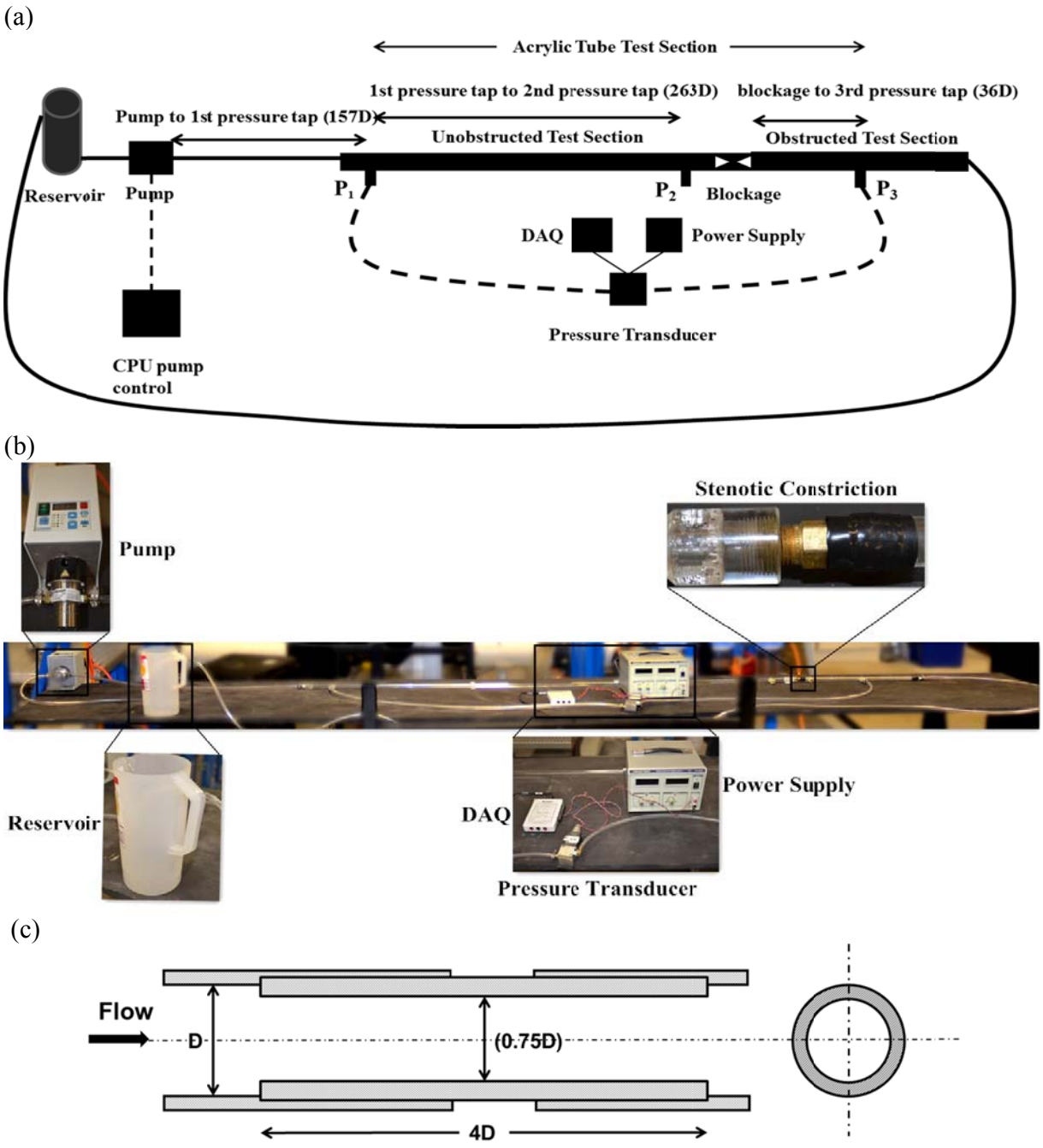

Figure 3.4 Schematic (a), photo (b) of the obstructed flow loop and schematic of the stenotic constriction (c) for steady and unsteady flow pressure drop measurements. Note that figure (a) is not drawn to scale.

Chapter Four: Results and Discussion

In this chapter, the results and discussions are presented in four main parts, namely steady unobstructed, pulsatile unobstructed, steady stenotic and pulsatile stenotic flows.

4.1 Steady Flow in Unobstructed Flow Loop

In order to validate the applicability of the existing theory to the experimental work, it is worthwhile to first carry out unobstructed steady flow measurements prior to the measurement of more complicated flows.

4.1.1 Pressure drop vs. Re

The transitional behaviours of the two analog fluids are presented by plotting measured pressure drop as a function of *Re* (Figure 4.1). The acquired measurements in laminar pipe flow were compared with Hagen-Poiseuille law (Equation 3.2) to check the validity of the current experimental work and to determine the Re_{cr} for the experimental setup.

As Figure 4.2 (a) shows, pressure drop displayed a linear increase until $Re \sim 2200$ for both analog fluids. At $Re \sim 2200$, pressure drop for the Newtonian fluid deviated from the laminar Hagen-Poiseuille relationship through $Re \sim 7600$ (Figure 4.2 (b, c)). This is in close agreement with the commonly accepted value of Re_{cr} in pipe flow, suggesting the suitability of the current experimental work; see Smits (2010), White (2011). Note that the standard deviations of the four total measurements at each *Re* were within 0.6% of each mean value and thus were not included in the displayed plots.

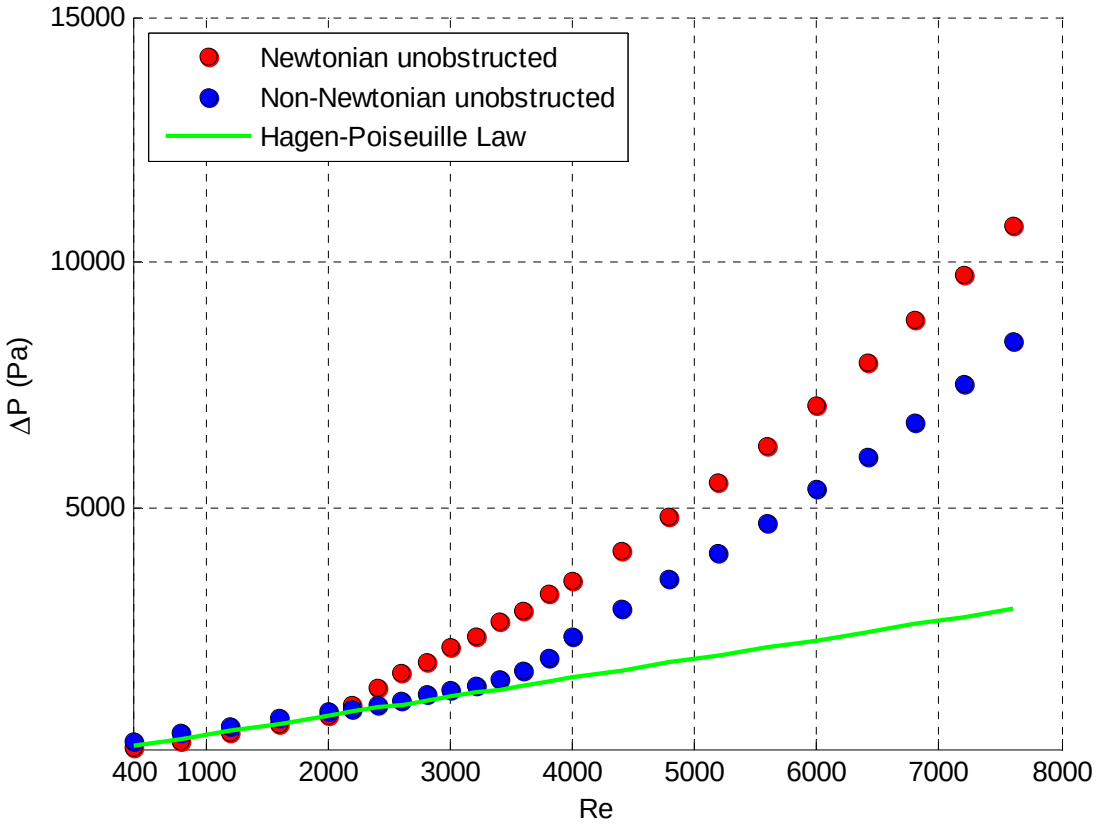

Figure 4.1 Measured pressure drop (ΔP) between P_1 and P_2 as a function of *Re* for the Newtonian and non-Newtonian analogs. The Hagen-Poiseuille Law is plotted for reference. Note that the standard deviations are within 0.6% of each mean value at every measurement point and thus not displayed in the plot.

In Figure 4.1, the pressure drop for the non-Newtonian analog is higher than the Newtonian counterpart at $400 < Re < 2000$. However, the error associated measurements at lower *Re* is high and thus little could be concluded in this region. Nevertheless, the higher pressure drop for the non-Newtonian analog suggests a higher level of energy dissipation in laminar flow. It is speculated that this behaviour is similar to that of red blood cells, where at low shear strain rates, the red blood cells form aggregates known as rouleaux and tumble while they flow along vessels, resulting in disturbed flow and a higher consumption of energy; see Ikbal et al. (2012).

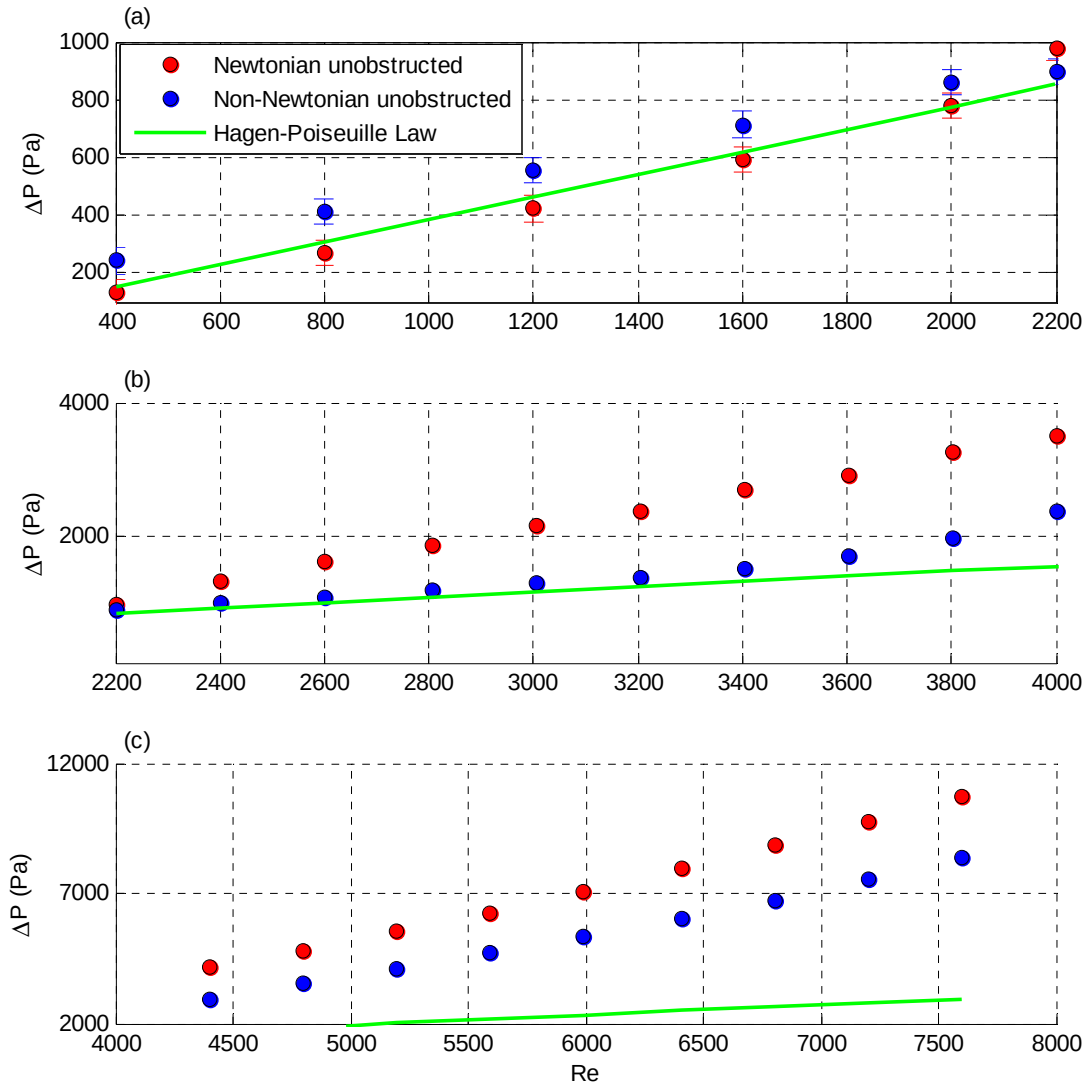

Figure 4.2 Measured pressure drop (ΔP) between P_1 and P_2 as a function of *Re* for the Newtonian and non-Newtonian analogs. The Hagen-Poiseuille Law is plotted for reference. Subplots: (a) pressure drop data for $400 < Re < 2000$, (b) pressure drop data for $2000 < Re < 4000$, and (c) pressure drop data for $4000 < Re < 7600$. Note that the errors bars in subplot (a) are due to the precision of the pressure transducer, which equates to a 44 Pa measurement error.

For the non-Newtonian blood analog, the pressure drops deviated from the Hagen-Poiseuille relation at $Re \sim 3200$, suggesting a delayed transition and prolonged laminar behaviour than the Newtonian analog. This is in qualitative agreement with Han et al. (2001), who reported that circulating porcine blood displayed laminar behaviour until $Re \sim 3200$ as compared to $Re \sim 2300$

for glycerol-water mixtures. This indicates that the viscoelastic and shear-thinning polymer xanthan gum solution suggested by Brookshier and Tarbell (1993) provides on a macroscale level a good representation of whole blood behaviour in transitional flow and its suitability for replicating blood behaviour in transitional flow. However, it was not the aim of this study to understand on the molecular level how the polymers could suppress turbulent bursts, but rather to gain insight into how blood would behave in transitional and turbulent regimes through the use of a blood analog containing polymers that mimic the non-Newtonian properties of blood; see Appendix 1. Nonetheless, it is proposed here that polymers, analogous to red blood cells, serve to dampen turbulent bursts and delay transition by deforming and orientating their long axis in the direction of flow. This delayed onset of transition measured for the blood mimicking non-Newtonian fluid suggests that the concept of blood being a purely viscous fluid is inadequate to predict the flow behaviour when modeling flow. Studies incorporating the Newtonian assumption of blood have ignored its visco-elasticity under the justification that the shear strain rates in large arteries are high enough for blood to be regarded as Newtonian; see Gijsen et al. (1999). However, based on the findings of the current study, the non-Newtonian effect of blood, predominantly in the form of visco-elasticity, should not be neglected due to the apparent difference shown by the two analog fluids at shear strain rates high enough whereupon Newtonian behaviour is often assumed, i.e. in transitional and turbulent regimes.

4.1.2 Moody diagrams

Combined with pressure drop measurements, a Moody diagram allowed for a direct comparison of both analog fluids in transitional and turbulent regimes. The prolonged laminar behaviour for the non-Newtonian analog fluid is confirmed by constructing a Moody diagram where f is plotted against Re. A good fit for both fluids to the laminar relation is seen in Figure

4.3 through $Re \sim 2200$. Upon an increase in Re, the Newtonian analog fluid shifted to the turbulent Blasius line, whereas the deviation is delayed to $Re \sim 3200$ for the non-Newtonian analog fluid. In turbulent pipe flow at $Re > 4000$, the non-Newtonian analog exhibited a lower pressure drop and f compared to its Newtonian counterpart seen in Figure 4.2 (c) and 4.3, which is known as the drag reduction phenomenon due to the polymer additive in the pure solvent; see Zadrazil et al. (2012). The error bars due to the precision of the pressure transducer is plotted in Appendix 1.

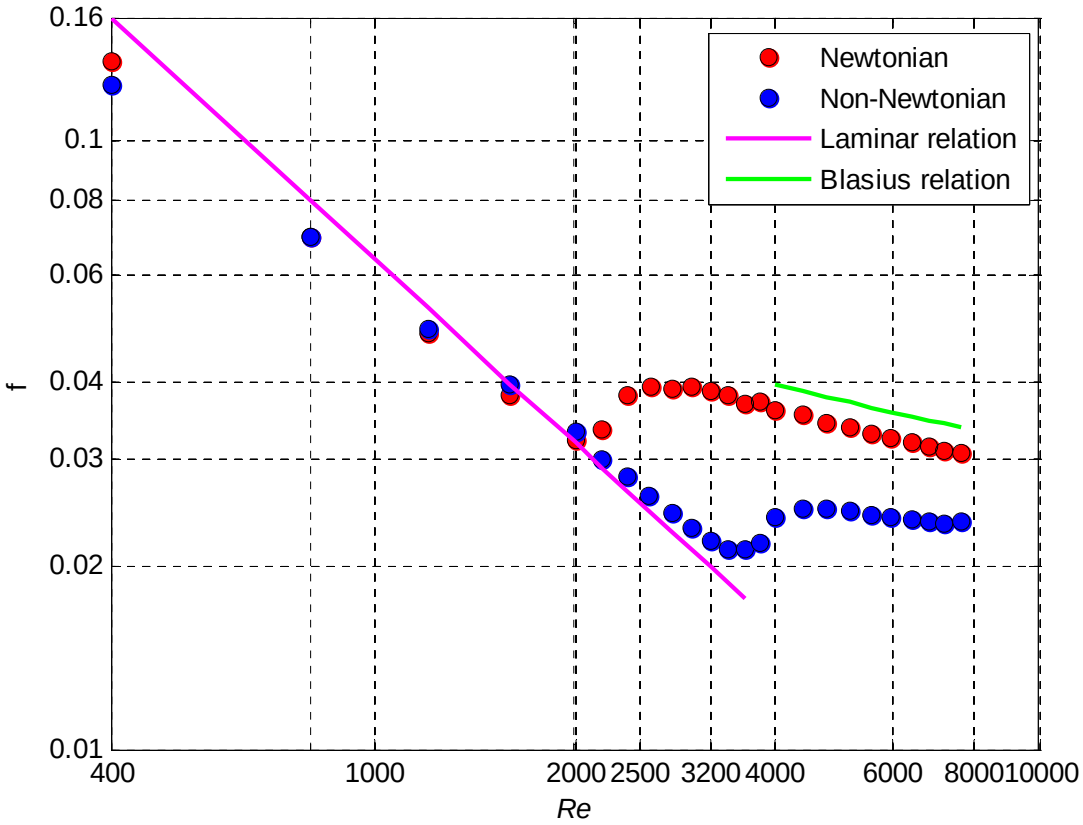

Figure 4.3 Moody diagram for steady flow of Newtonian and non-Newtonian analogs. The laminar Hagen-Poiseuille relationship ($f = 64/Re$) and the turbulent Blasius relationship ($f = 0.3164/Re^{1/4}$) have been plotted for reference.

Again, the different behaviours shown by the two analog fluids in transitional and turbulent flow emphasizes the importance of non-Newtonian viscous considerations through a delay of

transition that should be incorporated in the future modeling of arterial blood flow. However, when modeling laminar blood flow where shear strain rates exceed that of the shear-thinning range (> 400 s^{-1} in Figure 3.1), blood could be considered Newtonian since the behaviour of the non-Newtonian analog is comparable to that of the Newtonian analog in the laminar regime.\

4.2 Unsteady Flow in Unobstructed Flow Loop

The direct applicability of steady flow results to physiological problems is limited since blood flow in arteries is distinctly pulsatile. Since the transition characteristics of the current experimental system has been determined in the steady flow experiments as described earlier, I proceeded to measure the effects of a periodic flow component superimposed on a steady component and analyze its effects on transition. In this section, the effect of pulsatile frequency in the form of α on the initiation of transition for both fluids is analyzed.

4.2.1 Pressure drop vs. Re

Due to the general complexity of physiological pulsatile flow, primary quantitative results are limited to pressure drop characteristics of sinusoidal flow at α ~ 4 and 6. This is attained by firstly constructing plots of the time-averaged mean pressure drop (ΔP_m) as a function of Re_m at different α to directly evaluate the influence of pulsatile frequency on the transitional behaviour of both fluids. Pulsatile measurements were restricted to a Re_m of 5600 (peak *Re* of 7600) as a result of using an $AR = 1/3^{rd}$, which corresponded to the maximum flow rate of the attached pump head. It should be noted that although measurements at α~8 were initially intended to be acquired, the results were not repeatable due to pump performance limitations at high pulse frequency and thus were not included in the subsequent plots (see Appendix 1). Although the *in vivo* waveform of blood flow is not sinusoidal, the results obtained

with this simplified flow wave could nevertheless reveal the salient differences between the performances of the two blood analogs in unsteady flows.

Similar to steady flow behaviours, the non-Newtonian analog displayed a lower pressure drop in comparison to the Newtonian analog from Re_m ~ 2400 through Re_m ~ 5600, indicating that the added xanthan gum has a stabilizing effect on turbulence development in pulsatile flow as well. The α tested in this study fall in the range where Draad et al. (1998) found an increased sensitivity to a forced oscillatory disturbance for water after conversion of the dimensionless wave number of oscillatory flow to α. Although not the same polymer additive, the study by Draad et al. (1998) revealed that polymer solutions could withstand a larger forced oscillatory disturbance compared to water, which is in agreement with the findings in this section whereupon the mean pressure drop for the non-Newtonian analog fluid is lower than its Newtonian counterpart. On the other hand, they also identified that the polymers will reduce in general the natural transition Re_{cr}. However, the polymer additive used in the study of Draad et al. (1998) is polyacrylamide, which diminishes the direct comparability with the results presented here as it was found by Mann and Tarbell (1990) to exhibit highly elevated normal stresses in comparison to xanthan gum.

As Figure 4.4 shows, the mean pressure drop at α of 4 and 6 are comparable for both fluids, indicating that pulsatile frequency does not have an influence on the Re_{cr} for the onset of transition in pulsatile flow at these specific α. This is in contrast with the studies of Stettler and Hussian (1986) and Peacock et al. (1998). In the former, the researchers found that transition of Newtonian pulsatile flow is related to both Re_m and α, and that flow is stabilized (flow transitions at larger Re_{cr}) for $3 < \alpha < 10$ where the maximum stabilization occurs at α ~ 5. Similarly, in the latter, Peacock et al. (1998) reported that Re_{cr} is related to both Re_m and α through a power-law

relation across $1.5 < \alpha < 45$. Conversely, Trip et al. (2012) concluded that Re_{cr} is only dependent on Re_m for $\alpha > 10$. However, the studies by Stettler and Hussian (1986) and Trip et al. (2012) utilized a device to intentionally disturb the inlet flow prior to the measurement section, which may lower the Re_{cr} as in steady flow transition; see Peacock et al. (1998). Indeed, in the physiological system, the flow is not likely to be fully developed due to the curvatures and branching of vessels. However, this simplification is necessary if we are to conclude on the different behaviours of both analogs and to isolate the influence of visco-elasticity of the non-Newtonian analog in pulsatile pipe flow.

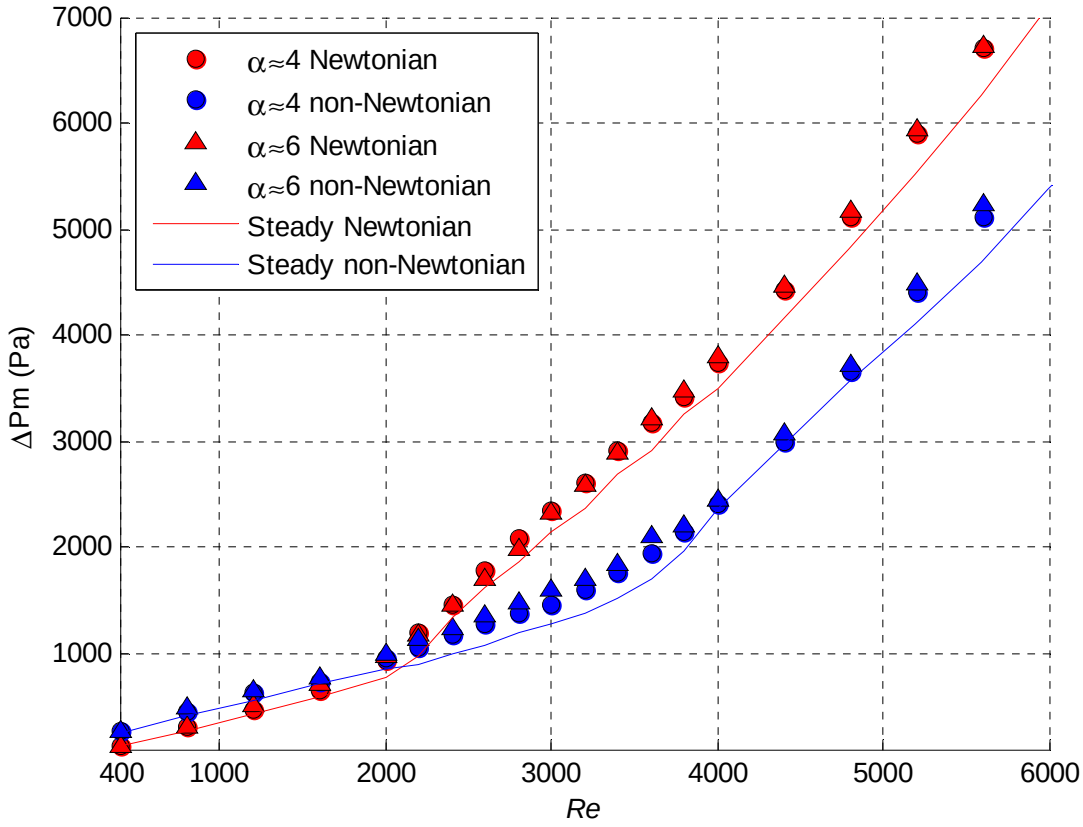

Figure 4.4 Measured time-averaged mean pressure drop between P_1 and P_2 under pulsatile conditions at α of ~ 4 and 6. Steady pressure drops for both analogs between P_1 and P_2 are plotted for comparison.

4.2.2 Moody diagrams

Moody diagrams were constructed to allow for a direct comparison of the response in transitional and turbulent pulsatile flow for both analog fluids as shown in Figure 4.5. The *f* for Newtonian pulsatile flow of α ~ 4 and 6 followed a roughly linear increasing trend until Re_m ~ 2000 whereupon it deviated from this laminar trend at Re_m ~ 2200. This indicates that the transition for pulsatile flow, i.e. small amplitude perturbations appearing in the decelerating and early accelerating phase of the velocity waveform, could be initiating between 2000 < Re_m < 2200; see Ohmi et al. (1982). In a thorough review by Carpinlioglu and Gundogdu (2001) on pulsatile transition of Newtonian fluids, they estimated that the critical Re_m for pulsatile flow is ~ 2100 based on existing findings. This further validates the current experimental work in carrying out pulsatile measurements. For the non-Newtonian analog, the *f* did not show a sharp deviation from its roughly linear trend until Re_m ~ 3800, which is higher than Newtonian pulsatile transition; see Figure 4.5. A similar mechanism to that presented for steady flow whereupon the added polymers stabilize flow and dampen instabilities is proposed here for the increased non-Newtonian pulsatile Re_{cr} compared to Newtonian pulsatile Re_{cr}.

On the other hand, for the non-Newtonian analog alone, it displayed a higher pulsatile Re_{cr} (~3800) than steady Re_{cr} (~3200). This implies that the stability of pulsatile non-Newtonian flow is increased in comparison to steady non-Newtonian flow through a further increase in prolonged laminar behaviour. This is in qualitative agreement with Thurston and Pope (1981), who concluded that the truncation of relaxation times of the polymers at high shear strain rates is responsible for the viscoelastic properties and that the onset of non-linearity with oscillatory flow occurs at higher shear strain rates than in steady flow. Based on their study, it is suggested that the different relaxation times of the polymers in the pulsatile cycle is responsible for a higher

pulsatile Re_{cr} than steady Re_{cr}; see Figure 4.4 and 4.6. It is inferred that the polymers were partly stretched at higher shear strain rate during the accelerating phase, whereupon they stretch slower or even partly retract during the decelerating phase, permitting the elastic energy to dissipate at a slower rate. Therefore, the same amount of elastic energy stored by the polymers could withstand a stable flow at a higher Re_m compared to steady flow.

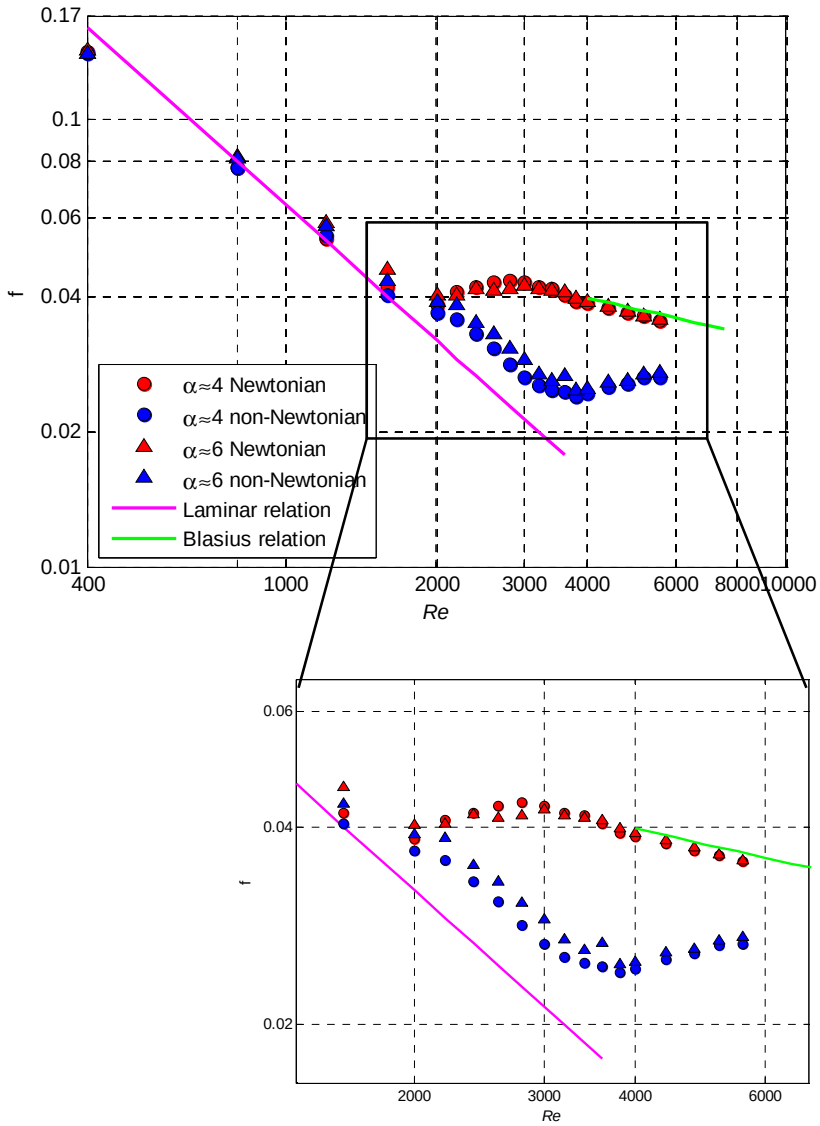

Figure 4.5 Moody diagram for pulsatile flow of two analog fluids at α of 4 and 6 between P_1 and P_2. Subplot: Moody diagram for $1600 < Re_m < 4000$ at different α. The laminar relation ($f = 64/Re$) and turbulent Blasius relation ($f = 0.316Re^{-0.25}$) are plotted for reference.

4.3 Obstructed Flow Loop

In shear layer induced turbulence downstream of a constriction in a pipe, the equation of *f* could no longer be properly applied to describe the frictional loss since *f* is only applicable to smooth pipes; see White (2011). In this section, the contribution of the added constriction and the turbulence energy dissipation (as in pressure drop) will be analyzed and compared between the two analog fluids as well as to the unobstructed model.

4.3.1 Steady flow

Given the addition of the stenotic constriction, pressure drops were acquired between P_1 and P_3 to determine the total obstructed system pressure drop. Figure 4.6 illustrates the total obstructed system pressure drop and the minor loss due to the introduction of the constriction for both analog fluids as described in Section 3.4.

For the axi-symmetric constriction used in the current study, the theoretical minor losses were also calculated using equations suggested by Seely and Young (1976) as follows using a similar constriction as with the current study (Figure 3.4 (c)):

$$\frac{\Delta P}{\rho U_0^2} = \frac{K_v}{\mathrm{Re}} + \frac{K_t}{2}\left[\frac{A_0}{A_1} - 1\right]^2 \tag{4.1}$$

$$K_v = 32\frac{L_a}{D_0}\left(\frac{A_0}{A_1}\right)^2 \tag{4.2}$$

$$L_a = 0.83L + 1.64D_1 \tag{4.3}$$

$$K_t = 1.52 \tag{4.4}$$

where ΔP is the pressure drop over the constriction, ρ is the density of the working fluid, U_0 is the inlet velocity, *Kv*, *Kt* and *La* the coefficients dependent of geometry, *Re* is the inlet Reynolds

number, A_0 is the inlet cross-sectional area, A_1 is the constricted cross-sectional area, D_0 is the inlet inner diameter, L is the length of the blunt plug and D_1 is the constricted inner diameter.

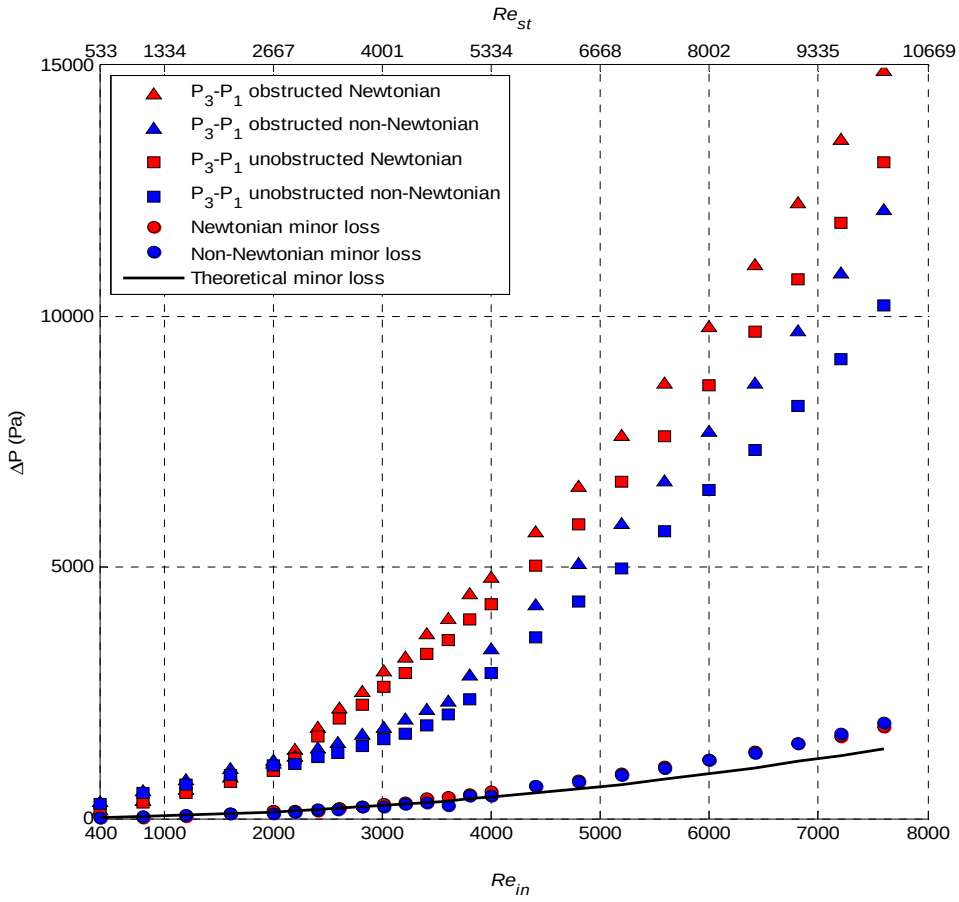

Figure 4.6 Total obstructed system pressure drops between P_1 and P_3 (triangle), expected unobstructed pressure drop between P_1 and P_3 (square) and minor losses and minor loss due to constriction (circle) for both analog fluids. Theoretical minor loss was calculated using Equations 4.1- 4.4 suggested by Seely and Young (1976). Re_{in} (Equation 3.15) and Re_{st} (Equation 3.16) have been plotted on the bottom and top y-axis, respectively.

It is observed in Figure 4.6 that for $400 < Re_{in} < 3000$, the above equations provide a good estimate for the minor losses. However, the equations underestimate the additional pressure drop due to the constriction at $Re_{in} > 3000$. It should be noted that in the work of Young and Tsai (1973a, b) and Seely and Young (1976), the experiments were restricted to a Re_{in} of 1000 with

Newtonian glycerol-water mixtures. Therefore, the equations were only applicable in the laminar recirculation region, whereas for transitional and turbulent post-stenotic flow, additional terms regarding the shear-layer induced instabilities and corresponding energy dissipation should be considered when evaluating minor losses.

The hex nipple attached to the unobstructed test section reduces the cross-sectional area and creates corresponding high velocities. When the fluid proceeds, it encounters a sudden area expansion and an emanating jet is formed. A sudden contraction and expansion could cause a marked pressure drop in the pipe because of both the increase in velocity and the loss of energy due to turbulence production; see Nichols and O'Rourke (2005). It is evident from previous studies that once a constriction is existent in the pipe, the flow will become less stable and transitions at a lower Re_{cr}; see Young and Tsai (1973a), Deshpande and Giddens (1980), Ahmed and Giddens (1983), Ojha et al. (1988), Siouffi (1997), Berger and Jou (2000), Beratlis et al. (2005), Blackburn and Sherwin (2007). The formation of strong shear layers downstream of the constriction is continuous at a random frequency and moves towards the pipe centerline until they eventually disappear as noted by Zadrazil et al. (2012). Oscillating shear stress is thus induced by vortices in the separated shear layer from the jet emerging from the constriction throat; see Pielhop et al. (2012). However, the specific values for Re_{cr} for shear layer induced convective instabilities are strongly dependent on the geometry of the constriction; see Young and Tsai, (1973a, b). Furthermore, as noted previously, studies quantifying blood flow, including stenotic flow field have largely relied on Newtonian assumptions. Tu and Deville (1996) considered the non-Newtonian effect of blood and concluded that the rheological properties of blood could significantly affect the flow in that non-Newtonian behaviour weakens the distortion of flow for mild stenosis (25% by area) and decreases the steady flow pressure drop for a larger

stenosis (75%). This is in accordance with Figure 4.6 in that the total pressure drops for the added constriction are less for the non-Newtonian analog than the Newtonian analog, similar to steady unobstructed flow results (see Section 4.1). The same mechanism is proposed here for the reduced pressure drop due to the visco-elasticity of the non-Newtonian analog. The polymers in the non-Newtonian fluid serve to dampen the turbulent bursts and reduce the possibility of shear layer induced vorticity formation downstream of the constriction, thus resulting in a lower pressure drop for the obstructed test section.

In order to show the difference between Newtonian and non-Newtonian analogs on the process of shear layer induced turbulence, ratios of the Newtonian to non-Newtonian pressure drop for the unobstructed system and the minor loss ratios are calculated as follows:

$$Percentage = \left[\left(\frac{\Delta P_{Nt}}{\Delta P_{non-Nt}} \right) - 1 \right] * 100\% \tag{4.5}$$

where ΔP_{Nt} represent either the Newtonian minor loss/unobstructed P_1 to P_2 pressure drops or the obstructed P_1 to P_3 pressure drops. ΔP_{non-Nt} represents corresponding non-Newtonian minor loss/unobstructed P_1 to P_2 pressure drops or the obstructed P_1 to P_3 pressure drops. Figure 4.7 displays the percentage difference in terms of pressure drop of the Newtonian to the non-Newtonian analog for both obstructed and unobstructed systems. It is observed that the ratios for the unobstructed system were higher across the measured Re_{in} and that the minor losses between two analogs were equivalent. Therefore, it could be deduced that the decreased obstructed system pressure drop ratios were due predominantly to the different viscous losses in the upstream unobstructed test section. Note that the data at $Re_{in} < 2000$ are associated with large errors due to the precision of the pressure transducer measurements at low pressure drops and thus are not displayed in subsequent figures.

Previous studies have revealed that a larger energy dissipation is associated with the downstream flow of a greater diameter sudden expansion, namely a larger upstream constriction; see Bullen et al. (1988), Fossa and Guglielmini (2002). Fratino and Pagano (2011) investigated the head loss coefficient that was found to be directly related to the energy dissipation of orifice plates with different diameters of reduction. Their study found that a larger recirculation length, recirculation height and head loss were associated with orifice plates of greater diameter reductions. This suggests that the loss of mechanical energy is relevant to the recirculating flow region whereupon longer recirculation lengths lead to higher levels of energy dissipation. In non-Newtonian post-stenotic flows, Pak et al. (1990) found that the non-Newtonian recirculation region is extended in transitional and turbulent flows. Similar observations were made by Walker et al. (2013). Although current data is not sufficient to draw definitive conclusions in detail, it is nonetheless proposed, based on previous findings, that the recirculation length in non-Newtonian post-stenotic flow is extended in transitional and turbulent flows, leading to an equivalent minor loss to Newtonian fluids. In light that the non-Newtonian analog dampens the convective instabilities as similar to that in the natural transition process, the comparable minor losses for both fluids would imply a longer recirculation length for the non-Newtonian analog in that the energy dissipation is related to flow reversal (see Figure 4.7). On the other hand, given the different ratios of pressure drop in natural transition and shear layer induced turbulence production, it could be suggested that when modelling unobstructed transitional/turbulent flow in large arteries, larger errors with regard to pressure drop are associated with the use of Newtonian assumptions of blood than modelling post-stenotic arterial flow.

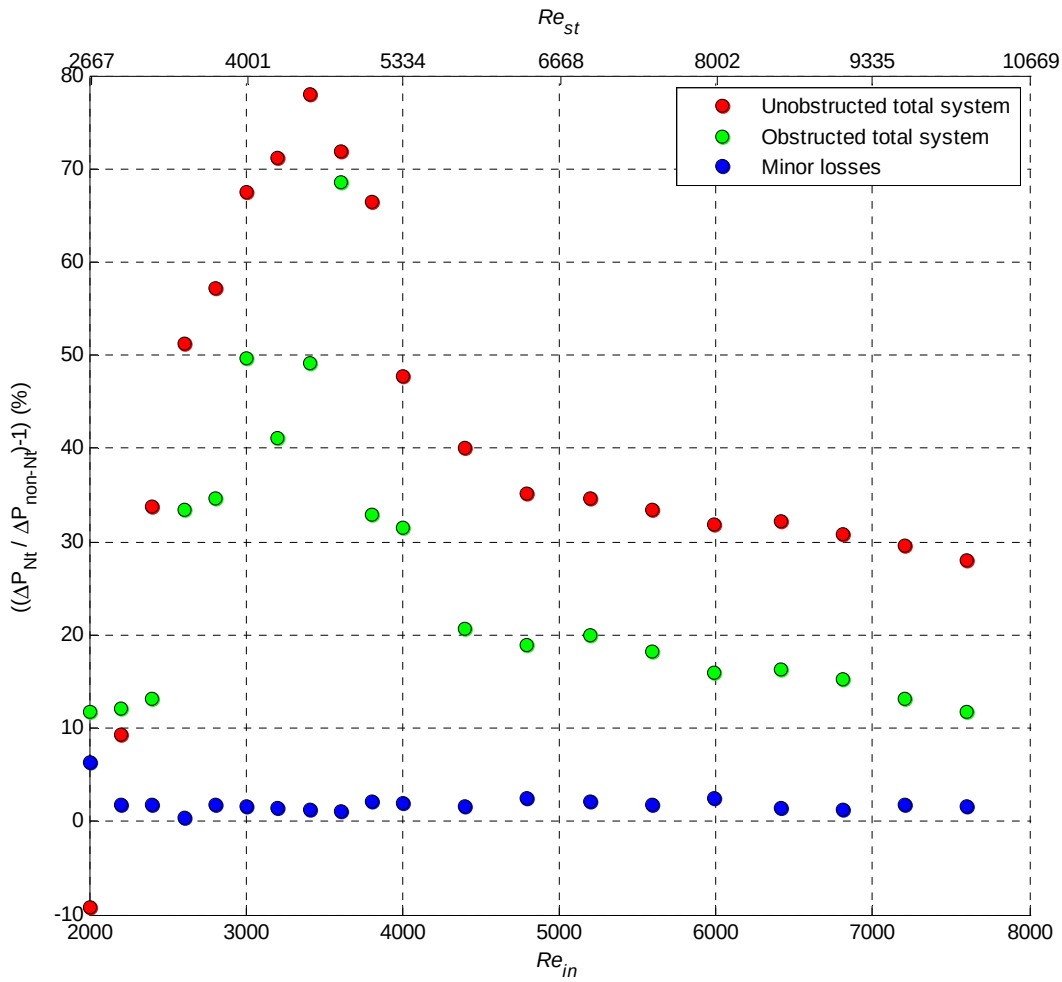

Figure 4.7 Ratios of the Newtonian (ΔP_{Nt}) to non-Newtonian pressure drops ($\Delta P_{non\text{-}Nt}$) for the unobstructed system (red), obstructed system (green) and Newtonian to non-Newtonian minor loss ratios in the obstructed system (blue). The ratios for the Newtonian to non-Newtonian pressure drops were much higher for the unobstructed system than the obstructed system while minor loss were comparable between the two fluids. Re_{in} (Equation 3.15) and Re_{st} (Equation 3.16) have been plotted on the bottom and top y-axis, respectively.

4.3.2 Unsteady flow

Similar to obstructed steady flow, the same analysis of the acquired pressure drop with the addition of the hex nipple and the second piece of acrylic pipe were performed for unsteady pulsatile flow after averaging and low pass filtering as described previously (see Section 3.3).

Figure 4.8 displays the total obstructed system pressure drops between P_1 and P_3 and the minor loss for both Newtonian and non-Newtonian analogs in matching dynamic conditions.

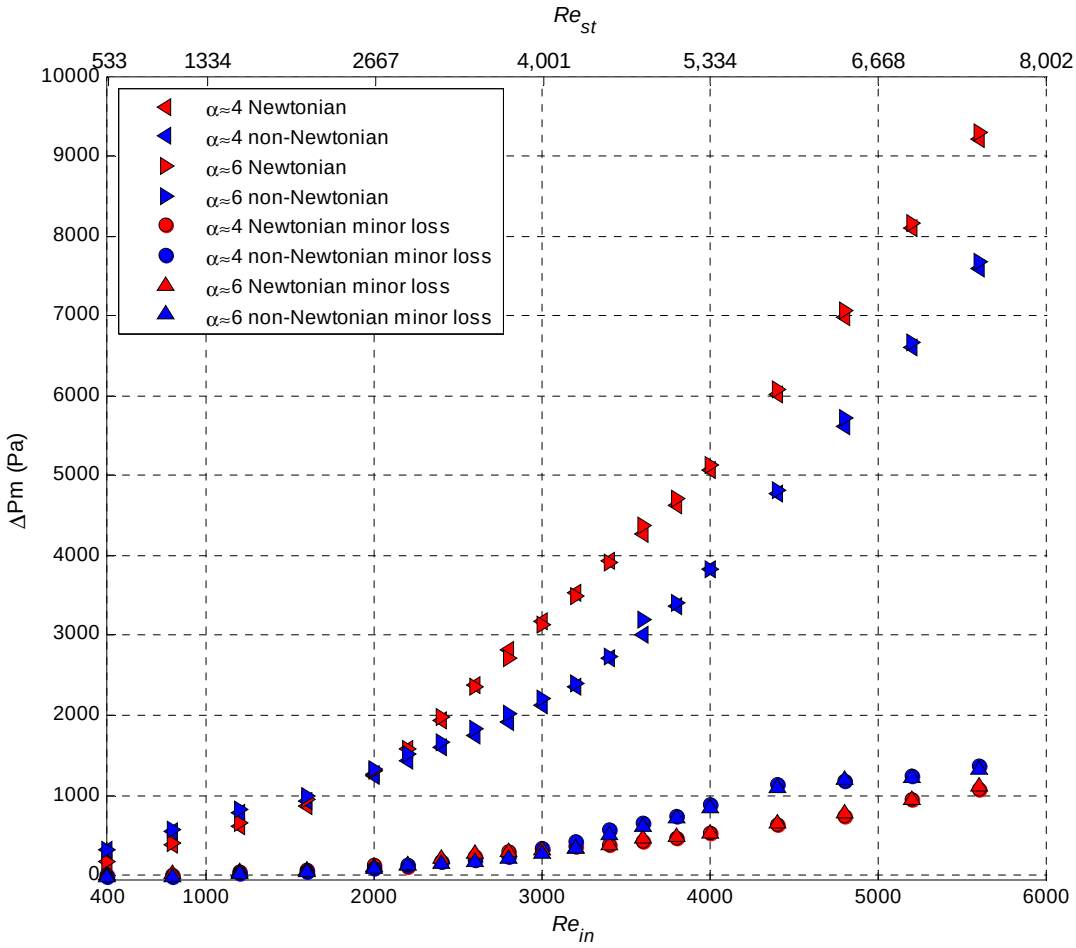

Figure 4.8 Total obstructed system pressure drops between P_1 and P_3, expected unobstructed pressure drop between P_1 and P_3 and minor losses for both analog fluids at α~4 and 6. Re_{in} (Equation 3.15) and Re_{st} (Equation 3.16) have been plotted on the bottom and top y-axis, respectively.

The total obstructed system pressure drops of the non-Newtonian analog were lower than those for the Newtonian analog as seen from Figure 4.8, which is similar to that observed with the steady obstructed flow results. This is in agreement with a computational study by Ikbal et al. (2012) using a visco-elastic model of a non-Newtonian fluid. It was found that the *f* for the visco-

elastic fluid was less than the Newtonian fluid in pulsatile flow. Pontrelli (2001) arrived at similar results of lowered pressure drop across the stenosis in pulsatile flow using non-Newtonian viscosity models. This further confirms the damping ability of the non-Newtonian analog and reemphasized the importance of the inclusion of non-Newtonian considerations when modelling blood flow.

In order to show the difference between Newtonian and non-Newtonian analogs on the process of shear layer induced turbulence in pulsatile flows, ratios of the Newtonian to non-Newtonian minor loss were compared with the unobstructed system pressure drop ratios as displayed in Figure 4.9. It is observed that the minor loss ratios were lower than the unobstructed system pressure drop ratios for $3000 < Re_{in} < 5600$ at both $\alpha \sim 4$ and 6. Based on an earlier argument for steady obstructed flow results, this could suggest that the recirculation lengths associated with pulsatile obstructed flow of the non-Newtonian fluid is longer in the transitional and turbulent regime. This would be in agreement with the findings of Walker et al. (2013) where they identified a similar trend for post-stenotic pulsatile flow of a non-Newtonian fluid at peak pulsatile flow of Re_{in} ~1250 and $\alpha \sim 4.4$. Similarly, Molla and Paul (2012) found an enlargement of the post-stenotic recirculation region using a non-Newtonian model in comparison to a Newtonian assumption.

Compared to steady flow ratios where minor losses were nearly equivalent across all *Re*, the minor loss ratios in pulsatile flow decreased whereupon non-Newtonian losses were greater than Newtonian losses between Re_{in} ~3400 to 5600 at both α values seen in Figure 4.9. This is inferred to be firstly due to the different relaxation times of the polymers as a result of the various shear strain rates experienced during pulsatile cycles as suggested by Thurston and Pope (1981). On the other hand, an even more prolonged recirculation region than non-Newtonian

steady flow recirculation could be expected to generate in light that polymers serve to stabilize the flow and delay pulsatile transition. The combined effects of the relaxation times and stabilized pulsatility contribute to a higher non-Newtonian pulsatile minor loss than steady non-Newtonian minor losses.

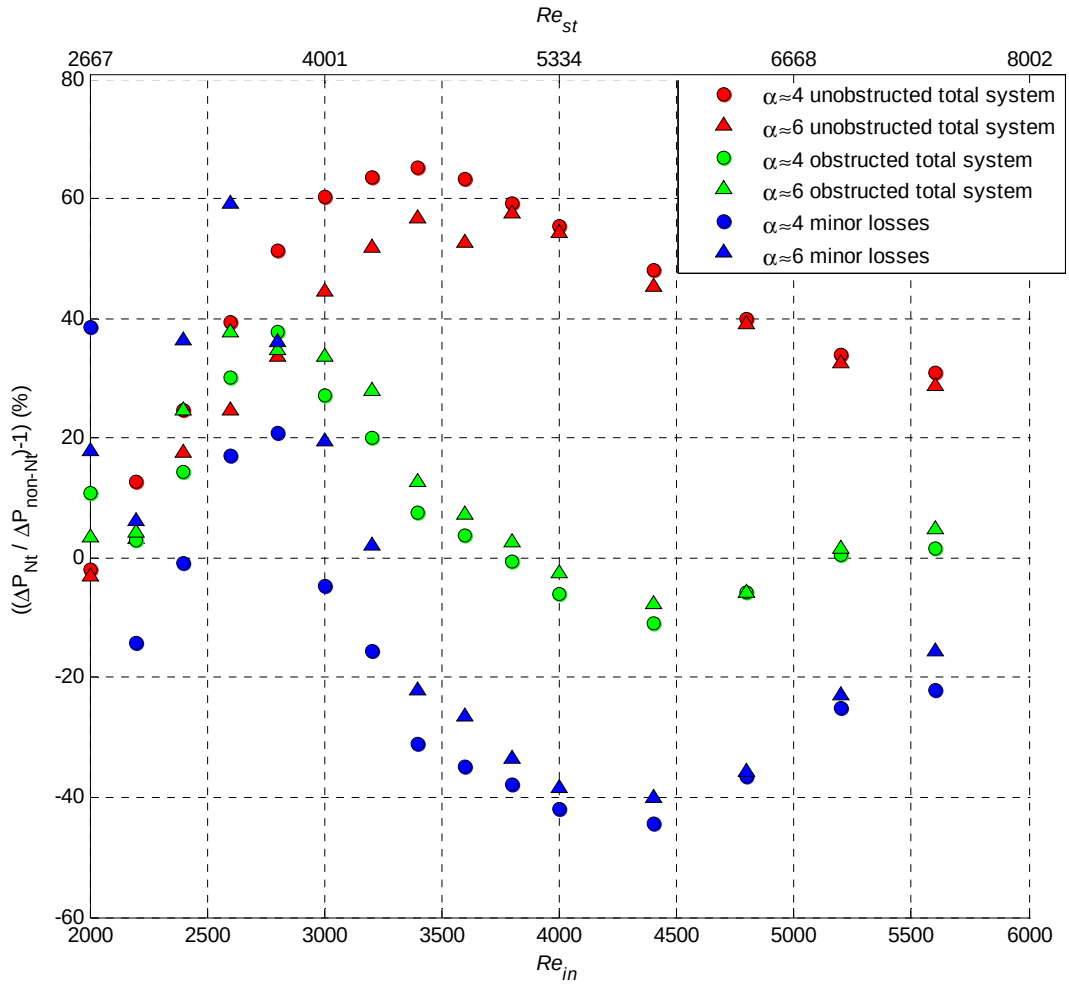

Figure 4.9 Ratios of the Newtonian (ΔP_{Nt}) to non-Newtonian mean pressure drops ($\Delta P_{non\text{-}Nt}$) for the unobstructed system (red), the obstructed system (green) and Newtonian to non-Newtonian minor loss ratios (blue) at α~4 and 6. The ratios of Newtonian/non-Newtonian pressure drops were lower for the minor loss than the unobstructed system in transitional/turbulent pulsatile flows. Re_{in} (Equation 3.15) and Re_{st} (Equation 3.16) have been plotted on the bottom and top y-axis, respectively.

Indeed, the complex flow features seen in the steady stenotic flow, when combined with pulsatility, can result in periodic transition in the deceleration phase more easily; see Varghese et al. (2007). However, it should be pointed out that computational modelling could be regarded as a validation for experimental results instead of accurately revealing physical mechanisms, since the post-stenotic flow is in its nature, extremely complex and thus cannot be fully explained by existing mathematical theories. On the other hand, given the different pressure drop ratios in obstructed and unobstructed unsteady flow, it could be deduced that greater pressure drop errors would accompany the modelling of unobstructed transitional/turbulent pulsatile flows in comparison to post-stenotic pulsatile flows.

4.4 Physiological Implications

The identification of turbulent and disturbed flow, and the conditions under which laminar or turbulent flow can exist in the cardiovascular system have long been of concern to physiologists as noted by Hershey and Im (1968). In humans with a normally functioning aortic valve and normal cardiac output, blood flow disturbances develop at peak velocity and persist into ejection and the decelerating phase with peak ascending aortic blood flow velocity ranging between 0.71 and 1.43 m/s; see Stein and Sabbah (1976). On the other hand, coarctations and stenosis provide examples of constrictions to blood flow where a stenosis is associated with cardiac murmurs that result from the noise created by the generation of turbulence in the jet downstream of the blockage; see Pedley et al. (2011). In patients with aortic valve stenosis, the level of turbulence is approximately 10 times that observed with normal human subjects with peak velocities ranging from 3.08 to 4.59 m/s, which equated to a peak *Re* of ~ 10,000; see Stein and Sabbah (1976). For flow downstream of an artificial heart valve, peak *Re* could reach 5000-

10,000; see Browne et al. (2000). Nerem et al. (1974) confirmed the existence of disturbed flow in the ascending aorta and descending thoracic aorta of dogs and horses. Furthermore, due to the natural curvature and narrowing of the vasculature and upstream perturbations, turbulence can be generated at Re_{in} as low as a few hundred depending on the severity of the stenosis; see Young and Tsai (1973a), Pedley et al. (2011). Therefore, turbulent blood flow is very likely to occur in both normal and diseased human. The average velocity range tested in this study is 0.085 m/s < $\overline{U}$ <1.61 m/s in steady flow and peak velocity of 0.11 m/s < $\overline{U}$ < 1.69 m/s in unsteady flow, which corresponds to the physiological range of the peak velocities observed in normal human ascending, descending aorta, patients with aortic valve stenosis or artificial mechanical heart valves and very likely patients with stenotic coronary and carotid artery; see Browne et al. (2000), Balducci et al. (2004), Pedley et al. (2011), Nguyen et al. (2012). The stenotic model used in the current study provides a first approximation to the physiological conditions where an emerging jet and shear layer induced turbulence would develop downstream of a blockage. The fundamental investigations of the non-linear behaviour of blood on the laminar-turbulent transition processes is essential in order to better understand the onset of turbulent blood flow and associated detrimental effects on vascular homeostasis.

In large arteries where the internal diameter is much larger compared to the size of the red blood cell, blood can be often be treated as a homogeneous Newtonian fluid with constant viscosity at all shear strain rates; see Nichols and O'Rourke (2005). However, the results presented in this study have demonstrated the importance of non-linear viscous considerations in modelling transitional and post-stenotic flows. It is proposed here based on past work that recirculation length is extended downstream of a stenosis with use of the non-Newtonian analog through the dampening behaviour of the added polymer whereupon a similar response is

expected if whole blood was used. This suggests that past work that has relied on Newtonian assumptions on post-stenotic flows may have underestimated the extent to which downstream endothelium is exposed to recirculation. Post-stenotic recirculation and instabilities are characterized by low and oscillatory WSS that have been proved to be responsible for the atherogenic phenotype of endothelial cells and resultant mechanisms that promote the progression of atherosclerosis. Regions of low and oscillatory WSS correspond to low nitric oxide production and enhanced arterial permeability, thus increasing the tendency for macromolecules, including low density lipoprotein to accumulate within the intima; see Nichols and O'Rourke (2005). However, due to the inverse relationship of shear strain rate and viscosity for shear-thinning fluids, past work has demonstrated that higher WSS would be measured when using non-linear viscous as opposed to Newtonian viscous assumptions; see Walker et al. (2012). Based on this, use of a Newtonian assumption for blood may not only underestimate the length of the recirculation region, it may also underestimate WSS levels that could lead to an overestimation of detrimental consequences to homeostatic mechanism as a result of low WSS in the recirculation region.

On the other hand, although turbulence is likely to be the cause of the progression of an arterial stenosis, it probably has little effect on atherogenesis; see Nichols and O'Rourke (2005), Pedley et al. (2011). The results in this study suggests that the deformation and flexibility of red blood cells provides the non-Newtonian behaviour of blood that serve to delay transition and dampen the generation of disturbance in conditions normally believed to trigger transition. Therefore, an earlier estimation of transition initiation using the Newtonian assumption of blood may have overemphasized the influence of turbulence on atherogenesis in healthy vessels.

Chapter Five: Conclusions and Recommendations

In this final chapter, the most important conclusions drawn from the studies presented are summarized first followed by a number of recommendations for future research.

5.1 Conclusions

In this study, pressure drop measurements for a circulating non-Newtonian blood analog were acquired in normal and stenotic *in vitro* arterial models to quantify the influence of non-Newtonian viscous behaviour on transition and turbulence initiation in comparison to a commonly used Newtonian analog. In general, it was found that the visco-elasticity of the non-Newtonian analog through the addition of an added polymer was likely responsible for the apparent difference in pressure–flow relationships compared to the Newtonian analog. It is suggested here that this is analogous on a macroscale level to the behaviour of red blood cells, which serve to prolong laminar flow behaviour that has been reported previously. Specific conclusions from this study include:

1. In a steady flow model representing a normal, healthy artery, results have shown that comparable and lower pressure drops were observed for the non-Newtonian analog in comparison to the Newtonian analog between $400 < Re < 2200$ and $2200 < Re < 7600$, respectively. For the Newtonian blood analog, transition occurred at the commonly accepted Re_{cr} of ~ 2200 while the non-Newtonian blood analog displayed prolonged laminar flow behaviour through $Re \sim 3200$, indicating a delayed initiation of transition.

It is speculated that, analogous to the non-Newtonian property of red blood cells, the visco-elastic polymers in the non-Newtonian blood analog served to dampen turbulent bursts and reduce the generation of instabilities in the natural transition process. One of the possible

mechanisms responsible for this behaviour is due to the elastic energy stored in the entangled polymers. It is suggested that this stored energy was released in transitional/turbulent flows under steady shear strain rates while the polymers orientated their long axis along the direction of flow, resulting in a lower energy dissipation (pressure drop) compared to the Newtonian analog. Furthermore, the close agreement of Re_{cr} for the non-Newtonian analog to that of porcine blood suggests the suitability of the xanthan gum blood analog to replicate whole blood behaviour when modelling transitional and turbulent flows.

2. In a pulsatile flow model of a healthy artery, the Newtonian analog showed a slightly smaller Re_{cr} and higher ΔP_m for pulsatile flow in comparison with steady flow. On the other hand, pulsatile frequency ($\alpha \sim 4$ and 6) does not appear to have an apparent influence on Newtonian flow behaviours. Further quantification is needed to draw broader conclusions regarding the controversial range of $4 < \alpha < 8$.

For non-Newtonian pulsatile flow, the visco-elastic polymers serve to decrease ΔP_m and delay transition compared to the Newtonian fluid through similar mechanisms in steady flow transition. Although the influence of pulsatile frequency on transition appears negligible at $\alpha \sim 4$ and 6, the non-Newtonian analog nonetheless exhibited a higher Re_{cr} compared to non-Newtonian steady transition. It is speculated that the different relaxation times exhibited for the visco-elastic polymers in pulsatile cycles allowed for a slower release of elastic energy, thus stabilizing the pulsatile flow until a larger Re_{cr}. It is further inferred that for other α between $4 < \alpha < 8$, the non-Newtonian analog would transition at a higher Re_{cr} than the Newtonian analog in that similar polymer dampening behaviours would be expected.

3. For the steady post-stenotic flow field, the non-Newtonian analog reduced the total obstructed pressure drop. However, the minor losses due to the presence of a constriction for the two analog fluids were equivalent. For the pulsatile post-stenotic flow field, the minor losses for the non-Newtonian analog were higher than the Newtonian analog.

Although not directly quantified, it is proposed based on previous studies that an extended recirculation length for the non-Newtonian fluid is responsible for the comparable minor loss with the Newtonian analog. It is speculated that by the extension of recirculation, the non-Newtonian analog reduces the generation of shear-layer induced instabilities downstream. For pulsatile flows, similar elongation of recirculation length was proposed for post-stenotic pulsatile flows whereupon the non-Newtonian minor losses exceeded Newtonian minor losses, specifically at $3400 < Re_{in} < 5600$ at both α measured. Furthermore, the varying shear strain rates during pulsatile cycles diminish the release of elastic energy by the polymers, which is suggested as a possible mechanism that led to increased non-Newtonian minor losses in relation to Newtonian. Thirdly, the increased stability, i.e. higher Re_{cr} observed in non-Newtonian unobstructed pulsatile flow, may contribute to the elongation of recirculation in the obstructed system. This finding could have a far-reaching effect on blood flow modelling that relies on Newtonian assumptions for the viscous behaviour of blood whereupon the extent of downstream stenotic recirculation may have been underestimated.

4. When modeling transitional and turbulent blood flow, the non-Newtonian viscous behaviour on account of the visco-elasticity of blood should be included as a modelled parameter. It was found, however, that the pressure drop / minor loss errors associated with the use of the Newtonian assumption were larger when modelling unobstructed steady and pulsatile arterial

blood flow in comparison to obstructed flow. However, the less pressure drop error due to the use of Newtonian assumption of blood does not imply smaller errors are associated with other flow metrics e.g. WSS or recirculation length downstream of the stenosis as well. The elongation of recirculation length suggested by past work and the current results indicates that the errors of modelled Newtonian downstream low and oscillatory WSS may still be large than if the non-Newtonian behaviour had been incorporated.

5.2 Future Recommendations

This study serves as a first approach to understand the transitional behaviour in experimentally modelled unobstructed and post-stenotic flows using a non-Newtonian blood analog. As noted previously, the physiological system is decidedly more complex than the models studied here and the non-Newtonian analog could only suggest a possible mechanism for the behaviour of red blood cells in those dynamic conditions. For a better understanding of blood flow in arteries, non-linear viscous assumptions together with other influencing factors such as vessel compliance and curvature could be included in the evaluation as well. Secondly, it would be useful to learn about the non-Newtonian viscous effect on triggered transition from a controlled disturbance instead of fully-developed inlet flow, since blood flow in the body is unlikely to be fully-developed due to natural curvatures and bending. Thirdly, this study only considered the influence of polymer visco-elasticity on post-stenotic flows. This could be expanded with regard to the shear-thinning behaviour in post-stenotic flow typical of low and oscillating WSS where past work has suggested an overestimation of post-stenotic low WSS using a Newtonian fluid; see Walker et al. (2012). Furthermore, for a more quantitative investigation of the process, it would be worthwhile to utilize flow visualization techniques such

as particle image velocimetry to measure for example the turbulent intensities and velocity profiles. Information on the whole flow field instead of a single point would detect the large- and small-scale coherent structures in the flow. It could also be used to verify the mechanisms proposed in this study as to whether the recirculation region is indeed extended for the non-Newtonian analog.

Appendix

Appendix 1. Limitations

1.1 Pump

Although measurements at $\alpha \sim 8$ were to be acquired, the step response of the pump was not sufficient to ensure repeatable data at higher pulsatile frequencies. Furthermore, the gear pump may cause mechanical degradation of the polymers in the non-Newtonian analog as a function of time, especially at higher Re/Re_m. Therefore, the non-Newtonian analog was disposed after the collection of measurements over the range of Re at which time a new, fresh analog was constructed and used for subsequent measurements. The same concentrations of glycerol, water and xanthan gum were used for each batch of the non-Newtonian analog to ensure consistency.

1.2 Experimental Setup

It should be noted that a number of simplifications were taken in this study to model the arterial flow. For example, the compliance of the arterial vessel wall and the natural curvature of vessel were neglected and the physiological arterial flow was represented by a sinusoidal waveform. The models used in this study must be considered, at best, a first approximation to the biological problem. However, the focus of this study was to emphasize the importance for the inclusion of non-linear viscous behaviour of blood in the future modeling of cardiovascular flow environments by investigating its specific influences on the process of transition and turbulent flow. Inclusion of the other non-linear physiologically appropriate parameters (e.g. compliant vessel wall) would make it difficult to isolate the contribution of the non-Newtonian behaviour on measured flow metrics. Given the purpose of this study, it is appropriate to investigate the problem first in simplified models before applying to more complex flow model systems.

Again, a number of simplifications are taken to model the arterial stenosis. Aside from the same simplifications used in the normal arterial model, natural irregularity and non-symmetric configuration of the physiological arterial stenosis was simplified to an axi-symmetric constriction. Although past work has shown that the determination of Re_{cr} for transition and turbulence is difficult due to the dependence of these critical values on the specific geometry of the constriction; see Young and Tsai (1973a,b), Seely and Young (1976), Vetel et al. (2008), the use of an axi-symmetric constriction to model arterial stenosis does not diminish the validity or importance of this study. The simplifications served to isolate the specific influence of the non-Newtonian viscous effects on the process of shear-layer induced turbulence and the results of this study could be applied to more complicated models which takes compliance for example into consideration.

1.3 Microscopic Behaviour of Xanthan Gum

The use of xanthan gum added to aqueous glycerol–water solution was used to replicate the rheological behaviour of whole blood on a macroscale level, in the hope that by using a blood analog, the behaviour of real, whole blood could be better understood. Therefore, it was not the goal of this study to investigate the behaviour of xanthan gum and to what degree it replicates red blood cell behaviour on a microscopic level. However, it is proposed that the deformable polymers in the solution is responsible for the drag reduction in turbulent flow and the elastic energy stored in the entangled polymers is dissipated by polymer stretching, thus reducing the overall dissipation of kinetic energy in a similar manner to that of red blood cells.

1.4 Errors in Voltage Measurements

The precision associated with the pressure transducer is 0.01 V, which equated to a +/- 44 Pa of measurement error. Although negligible at higher *Re*, large errors are associated with measurements at low *Re* in the laminar regime. The contribution of this measurement error to *f* is plotted in Figure 6.1 for unobstructed steady flow. Although the error associated with smaller *Re* is rather large, the laminar flow conditions were not of primary importance in this study other than providing comparisons with well-developed theory. For higher *Re* in the transitional and turbulent regimes, this measurement error became negligible and is of trivial importance to the apparent difference between the two fluids.

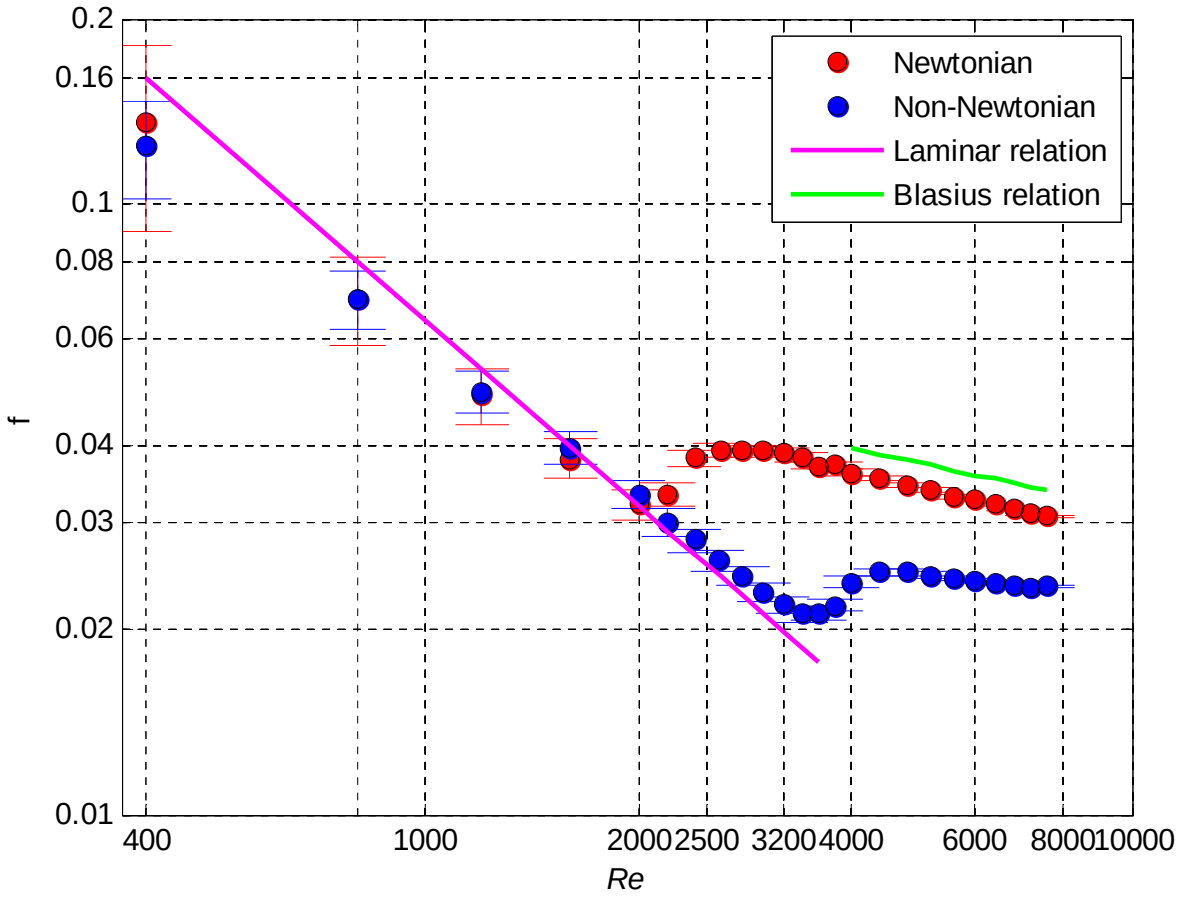

Figure 6.1 Error analysis of the *f* in unobstructed steady flow for both analog fluids. The laminar and turbulent relations are plotted for reference.

Appendix 2. Initial Tests

Initial pressure drop measurements with blood analogs of higher viscosities (~ 3.8cP) were acquired prior to the tests presented in Chapter 4. Initial blood analogs of greater viscosities were constructed following that suggested and tested by Brookshier and Tarbell (1993). The Newtonian control consisted of 40% by weight aqueous glycerol to match the asymptotic viscosity of the non-Newtonian fluid whereupon the non-Newtonian analog consisted of 0.025 wt. % xanthan gum and 30 wt. % glycerol. The viscosity of the Newtonian analog (3.8 cP) was acquired by a capillary viscometer with initial measurements made using water as a control fluid. The shear-thinning character of the non-Newtonian analog was also comparable to that of blood at selected hematocrit values. The working analog fluids were circulated through the same experimental setup in Figure 3.2. Identical pressure drop measurements were carried out across a range of *Re*. Based on the flow rate capabilities of the pump and the fluid viscosity, maximum *Re* for steady measurements was restricted to 3400. For pulsatile measurements, similar sinusoidal waveforms as Figure 3.3 were constructed to acquire pressure drop data for α ~3, 4.4 and 5 up to a maximum Re_m ~ 3000. Figure 6.2 and 6.3 illustrate the Moody diagrams for the initial steady and pulsatile measurements, respectively.

Similar results were observed with these initial fluids as compared to the results presented within the thesis itself. Transition initiation was delayed for the non-Newtonian analog to *Re* ~ 2800 whereas the Newtonian analog transitioned at *Re* ~ 2200. For pulsatile flow, Figure 6.3 shows little influence of α on the Re_{cr} for pulsatile flow of the two fluids and a lower *f* for the non-Newtonian analog. The initial steady non-Newtonian flow transitions at 2800 while pulsatile non-Newtonian flow still follows the laminar relation at Re_m~3000. This supports the prolonged laminar behaviour and stability of pulsatile non-Newtonian flow presented in Chapter 4.

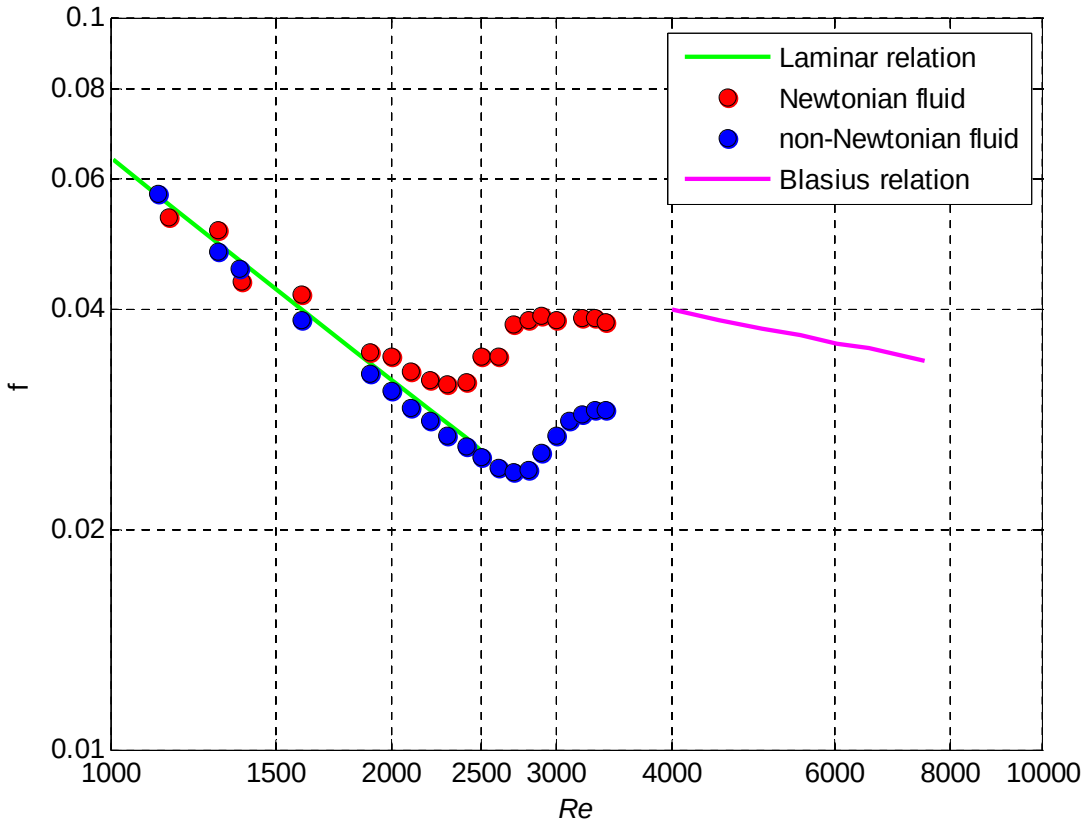

Figure 6.2 Moody diagram for the initial working analog fluids. The laminar Hagen-Poiseuille relationship (f=64/Re) and the turbulent Blasius relationship (f=0.3164/$Re^{1/4}$) for f and Re have been plotted for reference.

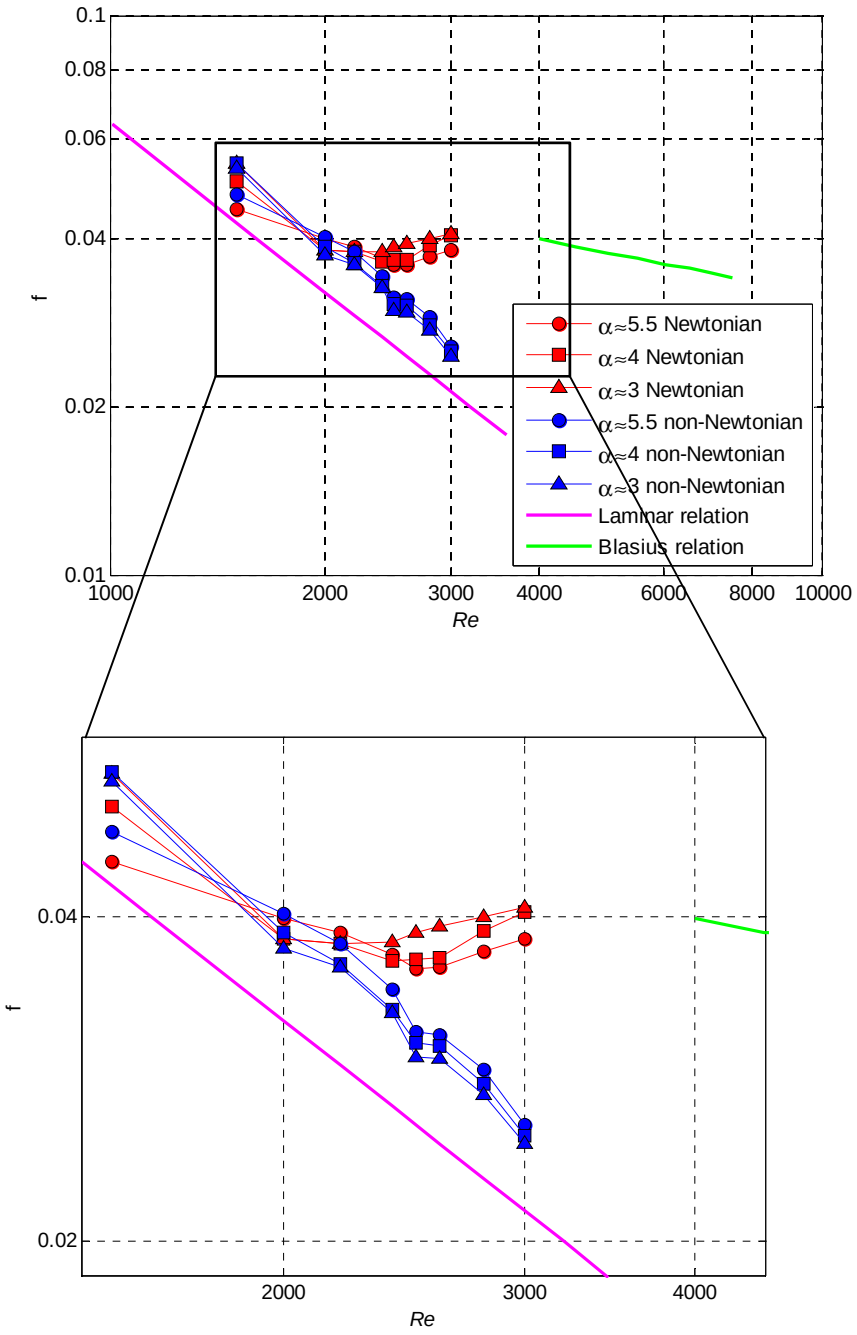

Figure 6.3 Combination of different α data of both Newtonian and non-Newtonian fluids. A certain region is magnified for clearer comparison the Newtonian fluid at different α. The Hagen-Poiseuille and Blasius relations are plotted here as reference.

Appendix 3. Repeatability Tests

Repeatability tests were carried out after acquiring the presented measurements on a separate day with refreshed blood analogs of the same composition as described in Section 4.2. The pressure drops at representative *Re* and Re_m in laminar, transitional and turbulent regimes for steady and pulsatile flows are presented in Figure 6.4 and 6.5, respectively. It can be observed that the measured (mean) pressure drops were repeatable for both fluids in the unobstructed and obstructed test sections and that the errors associated with larger flow rates in the transitional and turbulent regimes were within 5% of the corresponding (mean) pressure drops displayed in the results section.

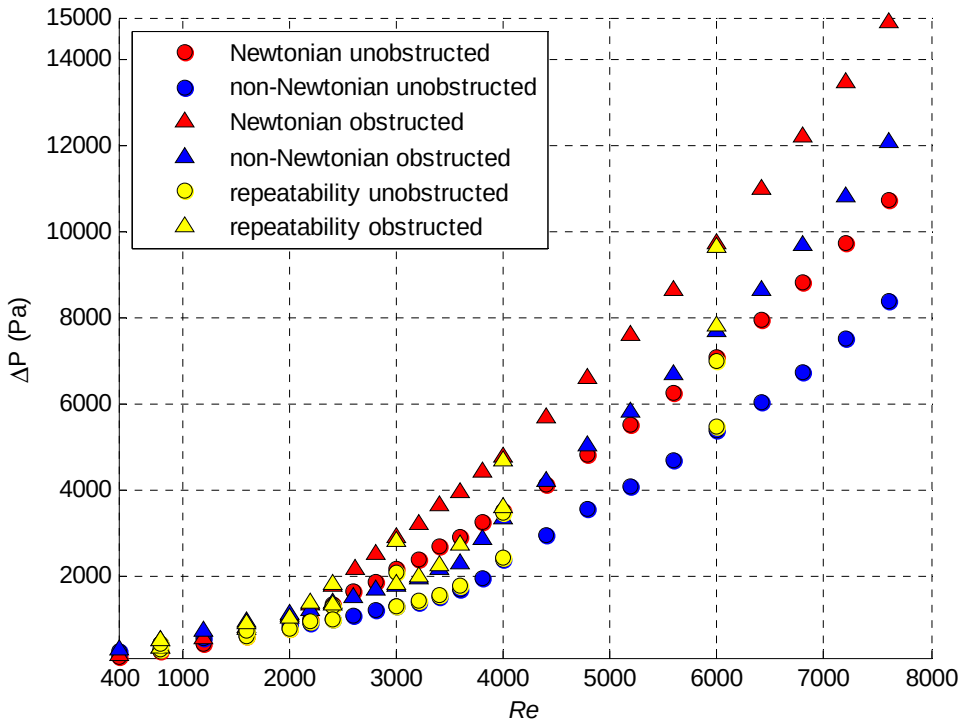

Figure 6.4 Repeated measurement for selected representative pressure drop for two analog fluids in laminar, transitional and turbulent regimes.

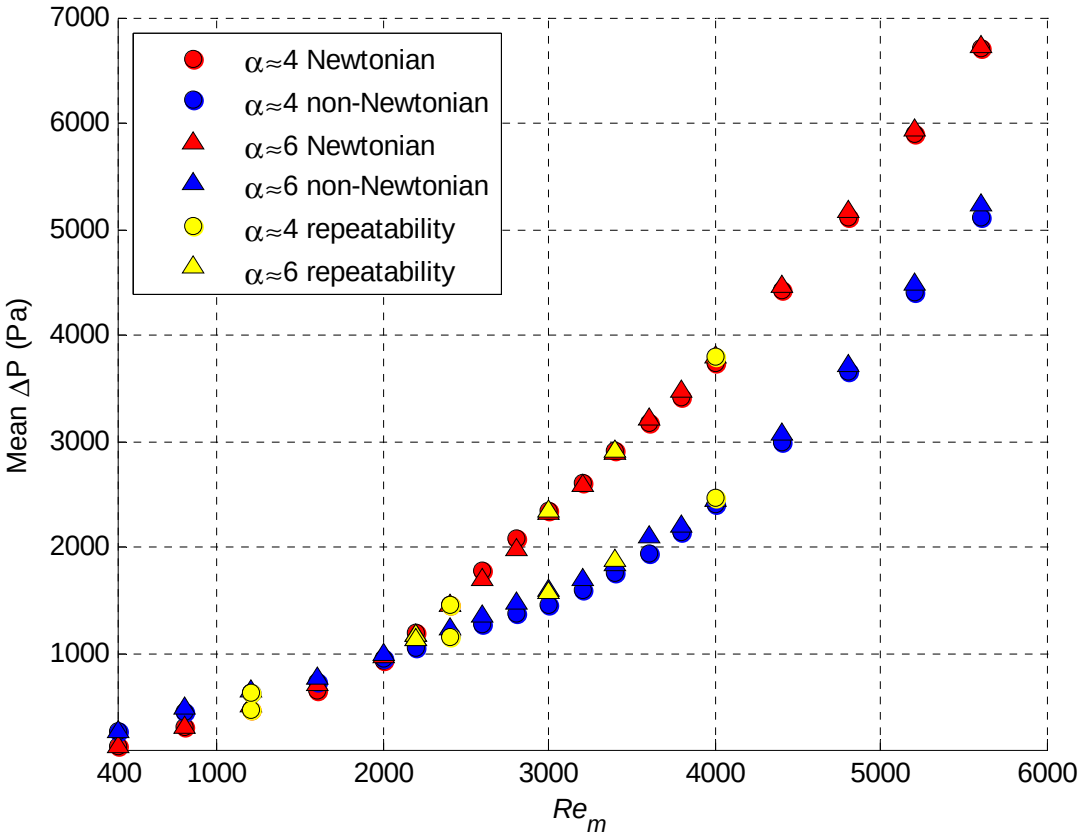

Figure 6.5 Repeated measurements for selected representative mean pressure drop for two analog fluids in laminar, transitional and turbulent regimes of pulsatile unobstructed flow.

References

Ahmed, S. A., & Giddens, D. P. (1983). Flow disturbance measurements through a constricted tube at moderate Reynolds numbers. *Journal of biomechanics*, *16*(12), 955-963.

Aoki, T., Wood, H. A., Old, L. J., & Boyse, E. A. (1969). Arterial wall shear and distribution of early atheroma in man. *Nature*, *223*(1), 159.

Ballyk, P. D., Steinman, D. A., & Ethier, C. R. (1994). Simulation of non-Newtonian blood flow in an end-to-end anastomosis. *Biorheology*, *31*(5), 65-586.

Balducci, A., Grigioni, M., Querzoli, G., Romano, G. P., Daniele, C., D'Avenio, G., & Barbaro, V. (2004). Investigation of the flow field downstream of an artificial heart valve by means of PIV and PTV. *Experiments in fluids*, *36*(1), 204-213.

Beratlis, N., Balaras, E., Parvinian, B., & Kiger, K. (2005). A numerical and experimental investigation of transitional pulsatile flow in a stenosed channel. *Journal of biomechanical engineering*, *127*(7), 1147-1157.

Berger, S. A., & Jou, L. D. (2000). Flows in stenotic vessels. *Annual Review of Fluid Mechanics*, *32*(1), 347-382.

Berman, N. S. (1978). Drag reduction by polymers. *Annual Review of Fluid Mechanics*, *10*(1), 47-64.

Bewersdorff, H. W., & Singh, R. P. (1988). Rheological and drag reduction characteristics of xanthan gum solutions. *Rheologica acta*, *27*(6), 617-627.

Blackburn, H. M., & Sherwin, S. J. (2007). Instability modes and transition of pulsatile stenotic flow: pulse-period dependence. *Journal of Fluid Mechanics*, *573*(1).

Blackburn, H. M., Sherwin, S. J., & Barkley, D. (2008). Convective instability and transient growth in steady and pulsatile stenotic flows. *Journal of Fluid Mechanics*, *607*(1), 267-277.

Brookshier, K. K., & Tarbell, J. M. (1991). Effect of hematocrit on wall shear rate in oscillatory flow: do the elastic properties of blood play a role?. *Biorheology*, *28*(6), 569.

Brookshier, K. A., & Tarbell, J. M. (1993). Evaluation of a transparent blood analog fluid: aqueous xanthan gum/glycerin. *Biorheology*, *30*(2), 107.

Browne, P., Ramuzat, A., Saxena, R., & Yoganathan, A. P. (2000). Experimental investigation of the steady flow downstream of the St. Jude bileaflet heart valve: a comparison between laser Doppler velocimetry and particle image velocimetry techniques. *Annals of biomedical engineering*, *28*(1), 39-47.

Bullen, P. R., Cheeseman, D. J., & Hussain, L. A. (1988). The effects of inlet sharpness on the pipe contraction pressure loss coefficient. *International journal of heat and fluid flow*, *9*(4), 431-433.

Cavalcanti, S. (1995). Hemodynamics of an artery with mild stenosis. *Journal of Biomechanics*, *28*(4), 387-399.

Chien, S. (1970). Shear dependence of effective cell volume as a determinant of blood viscosity. *Science*, *168*(3934), 977-979.

Cho, Y. I., & Kensey, K. R. (1990). Effects of the non-Newtonian viscosity of blood on flows in a diseased arterial vessel. Part 1: Steady flows. *Biorheology*, *28*(3-4), 241-262.

Chung, J. S., & Graebel, W. P. (1972). Laser Anemometer Measurements of Turbulence in Non-Newtonian Pipe Flows. *Physics of Fluids*, *15*, 546.

Darbyshire, A. G., & Mullin, T. (1995). Transition to turbulence in constant-mass-flux pipe flow. *Journal of Fluid Mechanics*, *289*, 83-114.

Deshpande, M. D., & Giddens, D. P. (1980). Turbulence measurements in a constricted tube. *Journal of Fluid Mechanics*, *97*, 65-89.

Dodge, D. W., & Metzner, A. B. (1959). Turbulent flow of non-newtonian systems. *AIChE Journal*, *5*(2), 189-204.

Draad, A. A., Kuiken, G. D. C., & Nieuwstadt, F. T. M. (1998). Laminar-turbulent transition in pipe flow for Newtonian and non-Newtonian fluids. *Journal of Fluid Mechanics*, *377*, 267-312.

Durst, F., Ray, S., Ünsal, B., & Bayoumi, O. A. (2005). The development lengths of laminar pipe and channel flows. *Journal of fluids engineering*, *127*(6), 1154-1160.

Einav, S., & Sokolov, M. (1993). An experimental study of pulsatile pipe flow in the transition range. *Journal of biomechanical engineering*, *115*(4A), 404.

Eckhardt, B., Schneider, T. M., Hof, B., & Westerweel, J. (2007). Turbulence transition in pipe flow. *Annu. Rev. Fluid Mech.*, *39*, 447-468.

Eckhardt, B. (2009). Introduction. Turbulence transition in pipe flow: 125th anniversary of the publication of Reynolds' paper. *Philosophical Transactions of the Royal Society A: Mathematical, Physical and Engineering Sciences*,*367*(1888), 449-455.

Fossa, M., & Guglielmini, G. (2002). Pressure drop and void fraction profiles during horizontal flow through thin and thick orifices. *Experimental Thermal and Fluid Science*, *26*(5), 513-523.

Fox, J. A., & Hugh, A. E. (1966). Localization of atheroma: a theory based on boundary layer separation. *British heart journal*, *28*(3), 388.

Fratino, U., & Pagano, A. (2011). Head loss coefficient of orifice plate energy dissipator. *Journal of Hydraulic Research*, *49*(6), 830-831.

Fry, D. L. (1968). Acute vascular endothelial changes associated with increased blood velocity gradients. *Circulation research*, *22*(2), 165-197.

Garcıa-Ochoa, F., Santos, V. E., Casas, J. A., & Gomez, E. (2000). Xanthan gum: production, recovery, and properties. *Biotechnology advances*, *18*(7), 549-579.

Geoghegan, P. H., Buchmann, N. A., Soria, J., & Jermy, M. C. (2013). Time-resolved PIV measurements of the flow field in a stenosed, compliant arterial model. *Experiments in Fluids*, *54*(5), 1-19.

Gijsen, F. J. H., Van de Vosse, F. N., & Janssen, J. D. (1999). The influence of the non-Newtonian properties of blood on the flow in large arteries: steady flow in a carotid bifurcation model. *Journal of biomechanics*, *32*(6), 601-608.

González, H. A., & Moraga, N. O. (2005). On predicting unsteady non-Newtonian blood flow. *Applied mathematics and computation*, *170*(2), 909-923.

Han, S. I., Marseille, O., Gehlen, C., & Blümich, B. (2001). Rheology of blood by NMR. *Journal of Magnetic Resonance*, *152*(1), 87-94.

Hershey, D., & Song, G. (1967). Friction factors and pressure drop for sinusoidal laminar flow of water and blood in rigid tubes. *AIChE Journal*, *13*(3), 491-496.

Hershey, D., & Im, C. S. (1968). Critical Reynolds number for sinusoidal flow of water in rigid tubes. *AIChE Journal*, *14*(5), 807-809.

Hof, B., Juel, A., & Mullin, T. (2003). Scaling of the turbulence transition threshold in a pipe. *Physical review letters*, *91*(24), 244502.

Hron, J., Málek, J., & Turek, S. (2000). A numerical investigation of flows of shear-thinning fluids with applications to blood rheology. *International journal for numerical methods in fluids*, *32*(7), 863-879.

Ikbal, MD. A., Chakravarty S.,SARIFUDDIN, & Mandal P. K. (2012). Unsteady Analysis of Viscoelastic Blood Flow through Arterial Stenosis. *Chem. Eng. Comm., 199*, 40-62.

Johnston, B. M., Johnston, P. R., Corney, S., & Kilpatrick, D. (2006). Non-Newtonian blood flow in human right coronary arteries: transient simulations. *Journal of biomechanics*, *39*(6), 1116-1128.

Liu, X., Fan, Y., Deng, X., & Zhan, F. (2011). Effect of non-Newtonian and pulsatile blood flow on mass transport in the human aorta. *Journal of biomechanics*, *44*(6), 1123-1131.

Lumley, J. L. (1969). Drag reduction by additives. *Annual review of fluid mechanics*, *1*(1), 367-384.

Málek, A. M, Largo, S., & Alper, S.L. (1999). Modulation by patho-physiological stimuli of the shear stress-induced up-regulation of endothelial nitric oxide synthase expression in endothlial cells. *Neurosurgury, 45,* 334-335.

Mann, D. E., & Tarbell, J. M. (1990). Flow of non-Newtonian blood analog fluids in rigid curved and straight artery models. *Biorheology*, *27*(5), 711.

Mejia, J., Mongrain, R., & Bertrand, O. F. (2011). Accurate prediction of wall shear stress in a stented artery: newtonian versus non-newtonian models. *Journal of biomechanical engineering*, *133*(7), 074501.

Mills, C. J., Gabe, I. T., Gault, J. H., Mason, D. T., Ross, J., Braunwald, E., & Shillingford, J. P. (1970). Pressure-flow relationships and vascular impedance in man. *Cardiovasc Res*, *4*(4), 405-417.

Mittal, R., Simmons, S. P., & Udaykumar, H. S. (2001). Application of large-eddy simulation to the study of pulsatile flow in a modeled arterial stenosis. *Journal of biomechanical engineering*, *123*(4), 325-332.

Molla, M. M., & Paul, M. C. (2012). LES of non-Newtonian physiological blood flow in a model of arterial stenosis. *Medical engineering & physics*, *34*(8), 1079-1087.

Mullin, T. (2011). Experimental studies of transition to turbulence in a pipe. *Annual Review of Fluid Mechanics*, *43*, 1-24.

Nerem, R. M., & Seed, W. A. (1972). An in vivo study of aortic flow disturbances. *Cardiovascular research*, *6*(1), 1-14.

Nguyen, V. T., Kuan, Y. H., Chen, P. Y., Ge, L., Sotiropoulos, F., Yoganathan, A. P., & Leo, H. L. (2012). Experimentally Validated Hemodynamics Simulations of Mechanical Heart Valves in Three Dimensions. *Cardiovascular Engineering and Technology*, *3*(1), 88-100.

Nichols, W. W., & O'Rourke, M. F. (2005). *McDonald's blood flow in arteries: theoretical, experimental, and clinical principles*. CRC Press.

Ohmi, M., Iguchi, M., & Urahata, I. (1982). Flow patterns and frictional losses in an oscillating pipe flow. *Bulletin of JSME*, *25*(202), 536-543.

Ojha, M., Cobbold, R. S., Johnston, K. W., & Hummel, R. L. (1989). Pulsatile flow through constricted tubes: an experimental investigation using photochromic tracer methods. *J. Fluid Mech*, *203*(1), 173-197.

Özdinç Çarpinlioğlu, M., & Yaşar Gündoğdu, M. (2001). A critical review on pulsatile pipe flow studies directing towards future research topics. *Flow Measurement and Instrumentation*, *12*(3), 163-174.

Pak, B., Cho, Y. I., & Choi, S. U. (1990). Separation and reattachment of non-Newtonian fluid flows in a sudden expansion pipe. *Journal of Non-Newtonian Fluid Mechanics*, *37*(2), 175-199.

Pak, B., Cho, Y. I., & Choi, S. U. (1991). Turbulent hydrodynamic behavior of a drag-reducing viscoelastic fluid in a sudden-expansion pipe. *Journal of non-newtonian fluid mechanics*, *39*(3), 353-373.

Peacock, J., Jones, T., Tock, C., & Lutz, R. (1998). The onset of turbulence in physiological pulsatile flow in a straight tube. *Experiments in fluids*, *24*(1), 1-9.

Pedley, T. J. (1980). *The fluid mechanics of large blood vessels* (Vol. 1). Cambridge: Cambridge University Press.

Pedley, T. J., Schroter, R. C., & Seed, W. A. (2011). *The Mechanics of the Circulation*. Cambridge University Press.

Pielhop, K., Klaas, M., & Schröder, W. (2012). Analysis of the unsteady flow in an elastic stenotic vessel. *European Journal of Mechanics-B/Fluids*, *35*, 102-110.

Pontrelli, G. (2001). Blood flow through an axisymmetric stenosis. *Proceedings of the Institution of Mechanical Engineers, Part H: Journal of Engineering in Medicine*, *215*(1), 1-10.

Poole, R. J., & Ridley, B. S. (2007). Development-length requirements for fully developed laminar pipe flow of inelastic non-Newtonian liquids. *Journal of Fluids Engineering*, *129*, 1281.

Pralhad, R. N., & Schultz, D. H. (2004). Modeling of arterial stenosis and its applications to blood diseases. *Mathematical biosciences*, *190*(2), 203-220.

Razavi, A., Shirani, E., & Sadeghi, M. R. (2011). Numerical simulation of blood pulsatile flow in a stenosed carotid artery using different rheological models. *Journal of biomechanics*, *44*(11), 2021-2030.

Sarpkaya, T. (1966). Experimental determination of the critical Reynolds number for pulsating Poiseuille flow. *Journal of Basic Engineering*, *88*, 589.

Sawyer, P. N. (Ed.). (1965). *Biophysical mechanisms in vascular homeostasis and intravascular thrombosis*. Appleton-Century-Crofts.

Schirmer, C. M., & Malek, A. M. (2007). Wall shear stress gradient analysis within an idealized stenosis using non-Newtonian flow. *Neurosurgery*, *61*(4), 853-864.

Seeley, B. D., & Young, D. F. (1976). Effect of geometry on pressure losses across models of arterial stenoses. *Journal of biomechanics*, *9*(7), 439-448.

Sherwin, S. J., & Blackburn, H. M. (2005). Three-dimensional instabilities and transition of steady and pulsatile axisymmetric stenotic flows. *Journal of Fluid Mechanics*, *533*, 297-327.

Siouffi, M., Deplano, V., & Pélissier, R. (1997). Experimental analysis of unsteady flows through a stenosis. *Journal of Biomechanics*, *31*(1), 11-19.

Smith, R. L., Blick, E. F., Coalson, J., & Stein, P. D. (1972). Thrombus production by turbulence. *Journal of applied physiology*, *32*(2), 261-264.

Smits, A. J. (2010). *Viscous Flows and Turbulence*, Princeton University.

Stein, P. D., & Sabbah, H. N. (1976). Turbulent blood flow in the ascending aorta of humans with normal and diseased aortic valves. *Circulation research*, *39*(1), 58-65.

Stein, P. D., Sabbah, H. N., & Mandal, A. K. (1976). Augmentation of sickling process due to turbulent blood flow. *Journal of Applied Physiology*, *40*(1), 60-66.

Stettler, J. C., & Hussain, A. K. M. (1986). On transition of the pulsatile pipe flow. *Journal of Fluid Mechanics*, *170*(1), 169-197.

Tang, D., Yang, C., Kobayashi, S., & Ku, D. N. (2004). Effect of a lipid pool on stress/strain distributions in stenotic arteries: 3-D fluid-structure interactions (FSI) models. *Journal of biomechanical engineering*, *126*(3), 363.

Taylor, C. A., & Draney, M. T. (2004). Experimental and computational methods in cardiovascular fluid mechanics. *Annu. Rev. Fluid Mech.*, *36*, 197-231.

Thurston, G. B., & Pope, G. A. (1981). Shear rate dependence of the viscoelasticity of polymer solutions.: II. xanthan gum. *Journal of Non-Newtonian Fluid Mechanics*, *9*(1), 69-78.

Tickner, E. G., & Sacks, A. H. (1969). Engineering simulation of the viscous behavior of whole blood using suspensions of flexible particles. *Circulation Research*, *25*(4), 389-400.

Trip, R., Kuik, D. J., Westerweel, J., & Poelma, C. (2012). An experimental study of transitional pulsatile pipe flow. *Physics of fluids*, *24*(1), 014103.

Tu, C., & Deville, M. (1996). Pulsatile flow of non-Newtonian fluids through arterial stenoses. *Journal of biomechanics*, *29*(7), 899-908.

Valant, A. Z., Žiberna, L., Papaharilaou, Y., Anayiotos, A., & Georgiou, G. C. (2011). The influence of temperature on rheological properties of blood mixtures with different volume expanders—implications in numerical arterial hemodynamics simulations. *Rheologica acta*, *50*(4), 389-402.

Varghese, S. S., Frankel, S. H., & Fischer, P. F. (2007). Direct numerical simulation of stenotic flows. Part 2. Pulsatile flow. *Journal of Fluid Mechanics*, *582*, 281-318.

Vétel, J., Garon, A., Pelletier, D., & Farinas, M. I. (2008). Asymmetry and transition to turbulence in a smooth axisymmetric constriction. *Journal of Fluid Mechanics*, *607*, 351-386.

Virk, P. S., Merrill, E. W., Mickley, H. S., Smith, K. A., & Mollo-Christensen, E. L. (1966). *The Toms phenomenon: turbulent pipe flow of dilute polymer solutions* (Doctoral dissertation, Massachusetts Institute of Technology).

Virk, P. S. (1975). Drag reduction fundamentals. *AIChE Journal*, *21*(4), 625-656.

Walker, A. M., Johnston, C. R., & Rival, D. E. (2012). The Quantification of Hemodynamic Parameters Downstream of a Gianturco Zenith Stent Wire Using Newtonian and non-Newtonian Analogue Fluids in a Pulsatile Flow Environment. *Journal of biomechanical engineering*, *1*, 484.

Walker, A. M., Johnston, C. R., & Rival, D. E. (2013). On the Characterization of a Non-Newtonian Blood Analog and Its Response to Pulsatile Flow Downstream of a Simplified Stenosis. *Annals of biomedical engineering*, 1-13.

Willis, A. P., Peixinho, J., Kerswell, R. R., & Mullin, T. (2008). Experimental and theoretical progress in pipe flow transition. *Philosophical Transactions of the Royal Society A: Mathematical, Physical and Engineering Sciences*,*366*(1876), 2671-2684.

White, F. M. (2010). *Fluid Mechanics (7th Ed.)*. McGraw Hill.

Wygnanski, I. J., & Champagne, F. H. (1973). On transition in a pipe. Part 1. The origin of puffs and slugs and the flow in a turbulent slug. *Journal of Fluid Mechanics*, *59*(02), 281-335.

Yee, A., Bosworth, K. A., Conway, D. E., Eskin, S. G., & McIntire, L. V. (2008). Gene expression of endothelial cells under pulsatile non-reversing vs. steady shear stress; comparison of nitric oxide production. *Annals of biomedical engineering*, *36*(4), 571-579.

Young, D. F., & Tsai, F. Y. (1973a). Flow characteristics in models of arterial stenoses—I. Steady flow. *Journal of biomechanics*, *6*(4), 395-410.

Young, D. F., & Tsai, F. Y. (1973b). Flow characteristics in models of arterial stenoses—II. Unsteady flow. *Journal of biomechanics*, *6*(5), 547-559.

Zadrazil, I., Bismarck, A., Hewitt, G. F., & Markides, C. N. (2012). Shear layers in the turbulent pipe flow of drag reducing polymer solutions. *Chemical Engineering Science*, *72*, 142-154.

Zakin, J. L., Ni, C. C., Hansen, R. J., & Reischman, M. M. (1977). Laser Doppler velocimetry studies of early turbulence. *Physics of Fluids*, *20*, S85.